Plant Physiology and Biochemistry 226 (2025) 110067

Contents lists available at ScienceDirect

Plant Physiology and Biochemistry

journal homepage: www.elsevier.com/locate/plaphy

Coclaurine *N*-methyltransferase-like enzymes drive the final biosynthetic reaction of the anti-Alzheimer's drug galanthamine in Amaryllidaceae

Nuwan Sameera Liyanage [a], Basanta Lamichhane [a], Elisa Fantino [a], Natacha Mérindol [a], Sarah-Eve Gélinas [a], Maria Camila García Tobón [a], Isabel Desgagné-Penix [a,b,*]

[a] Department of Chemistry, Biochemistry and Physics, Université du Québec à Trois-Rivières, Trois-Rivières, QC, Canada
[b] Plant Biology Research Group, Trois-Rivières, Québec, Canada

ARTICLE INFO

Keywords:
Alkaloids
Norgalanthamine
Specialized metabolism
Hippeastrum papilio
Leucojum aestivum
Lycoris radiata
Substrate promiscuity
Molecular docking
Environmental stress

ABSTRACT

Galanthamine, an isoquinoline alkaloid used to treat symptoms of Alzheimer's disease, is predominantly extracted from Amaryllidaceae plants, yet its supply remains limited. In this study, we identified, isolated, and characterized *N*-methyltransferases (NMTs) from three galanthamine-producing species: *Leucojum aestivum*, *Lycoris radiata*, and *Hippeastrum papilio*. The transcriptomic analysis identified five unique NMT isoforms, among which *LaLrHp*NMT1, an isoform highly conserved across all three species, exhibited the highest catalytic activity. Phylogenetic and structural analyses revealed that these enzymes share high sequence conservation and maintain the class I methyltransferase Rossmann fold with key catalytic residues, paralleling known NMTs from benzylisoquinoline alkaloid pathways. Flexible docking simulations confirmed that norgalanthamine, a crucial precursor, fits within the enzyme's active site and interacts with conserved residues Glu204 and His208. *In vitro* and *in planta* assays demonstrated that *LaLrHp*NMT1 efficiently catalyzes the *N*-methylation of norgalanthamine to galanthamine. Site-directed mutagenesis confirmed the key role of Glu204 and the participation of Phe residues in substrate stabilization. Additional enzyme assays revealed that *LaLrHp*NMT1 is promiscuous towards various alkaloid intermediates, while subcellular localization using eGFP-tagged constructs exposed a dual distribution in the cytosol and endoplasmic reticulum, suggesting that NMT activity occurs at the cytosol–ER interface where other biosynthetic enzymes reside. Environmental stress experiments in *H. papilio* shoots culture showed significant upregulation of *NMT* expression under heat and other stress conditions associated with AA levels modulation, indicating a potential link between stress responses and alkaloid biosynthesis. These findings deepen our understanding of galanthamine biosynthesis and provide a foundation for metabolic engineering strategies aimed at improving production yields.

1. Introduction

In the 1950s, a Russian scientist identified galanthamine, a plant isoquinoline alkaloid (*aka* Amaryllidaceae alkaloid (AA)) from *Galanthus woronowii*, after observing its traditional use in treating poliomyelitis (Heinrich and Lee Teoh, 2004). Galanthamine's anticholinesterase activity and neuromuscular blocking antagonism led to its approval for Alzheimer's treatment in over 32 countries (Loy and Schneider, 2006; Olin and Schneider, 2002; Hotchandani and Desgagne-Penix, 2017). The Amaryllidoideae subfamily produces over 700 AAs with diverse biological activities, including anti-cancer, anti-viral, anti-inflammatory, and antioxidant (Berkov et al., 2020; Ding et al., 2017; Jayawardena et al., 2024; Ka et al., 2020; He et al., 2015; Merindol et al., 2024). As galanthamine and other AAs in the pharmaceutical industry are primarily sourced from plants, understanding the enzymatic steps of their biosynthesis offers biotechnological opportunities to enhance their production.

The biosynthesis of AAs involves complex enzymatic steps, some elucidated and others yet to be uncovered. This process begins with aromatic amino acids, tyrosine, and phenylalanine, which produce precursors leading to norbelladine (Desgagné-Penix, 2021; Jayawardena et al., 2024) (Fig. 1). The enzymes norbelladine synthase (NBS) and noroxomaritidine/norcraugsodine reductase (NR), studied in species such as *Narcissus* spp. and *Leucojum aestivum*, catalyze the condensation of 3,4-dihydroxybenzaldehyde and tyramine to form norbelladine, indicating the start of the main AA biosynthetic pathway

* Corresponding author. Department of Chemistry, Biochemistry and Physics, Université du Québec à Trois-Rivières, Trois-Rivières, QC, Canada.
E-mail address: Isabel.Desgagne-Penix@uqtr.ca (I. Desgagné-Penix).

https://doi.org/10.1016/j.plaphy.2025.110067
Received 12 February 2025; Received in revised form 19 May 2025; Accepted 21 May 2025
Available online 22 May 2025

(Majhi et al., 2023; Tousignant et al., 2022; Singh et al., 2018; Kilgore et al., 2016). Norbelladine *O*-methyltransferase (NOMT) then methylates norbelladine at specific hydroxyl groups (Li et al., 2019; Koirala et al., 2024; Kilgore et al., 2014). NOMT has been examined in various species, including *Narcissus* spp. and *Lycoris* spp., finding species-specific differences in enzyme activity and substrate selectivity (Wang et al., 2024; Sun et al., 2018; Li et al., 2019; Koirala et al., 2024). 4′-*O*-methylnorbelladine, a branchpoint intermediate in the pathway, is then modified by various enzymes, contributing to the structural diversity of AAs. CYP96T1 from *Narcissus pseudonarcissus* predominantly catalyzes *para–para'* coupling, with minor *para–ortho*' phenol coupling (Kilgore et al., 2016a, b). Additional CYP96T enzymes identified in *Narcissus* cv. Tête-à-Tête, *Lycoris aurea,* and *L. aestivum* catalyze diverse phenol coupling reactions (Mehta et al., 2024; Liu et al., 2024; Lamichhane et al., 2025). Nornarwedine, the *para-ortho'* product, undergoes *N*-methylation via tocopherol *N*-methyltransferase (TocoNMT) to yield narwedine, which is reduced to galanthamine by an aldoketo reductase (AKR) (Mehta et al., 2024) (Fig. 1). While TocoNMT cannot methylate norgalanthamine to galanthamine (Mehta et al., 2024), radio- and stable-isotope labeling studies suggest multiple biosynthetic routes for

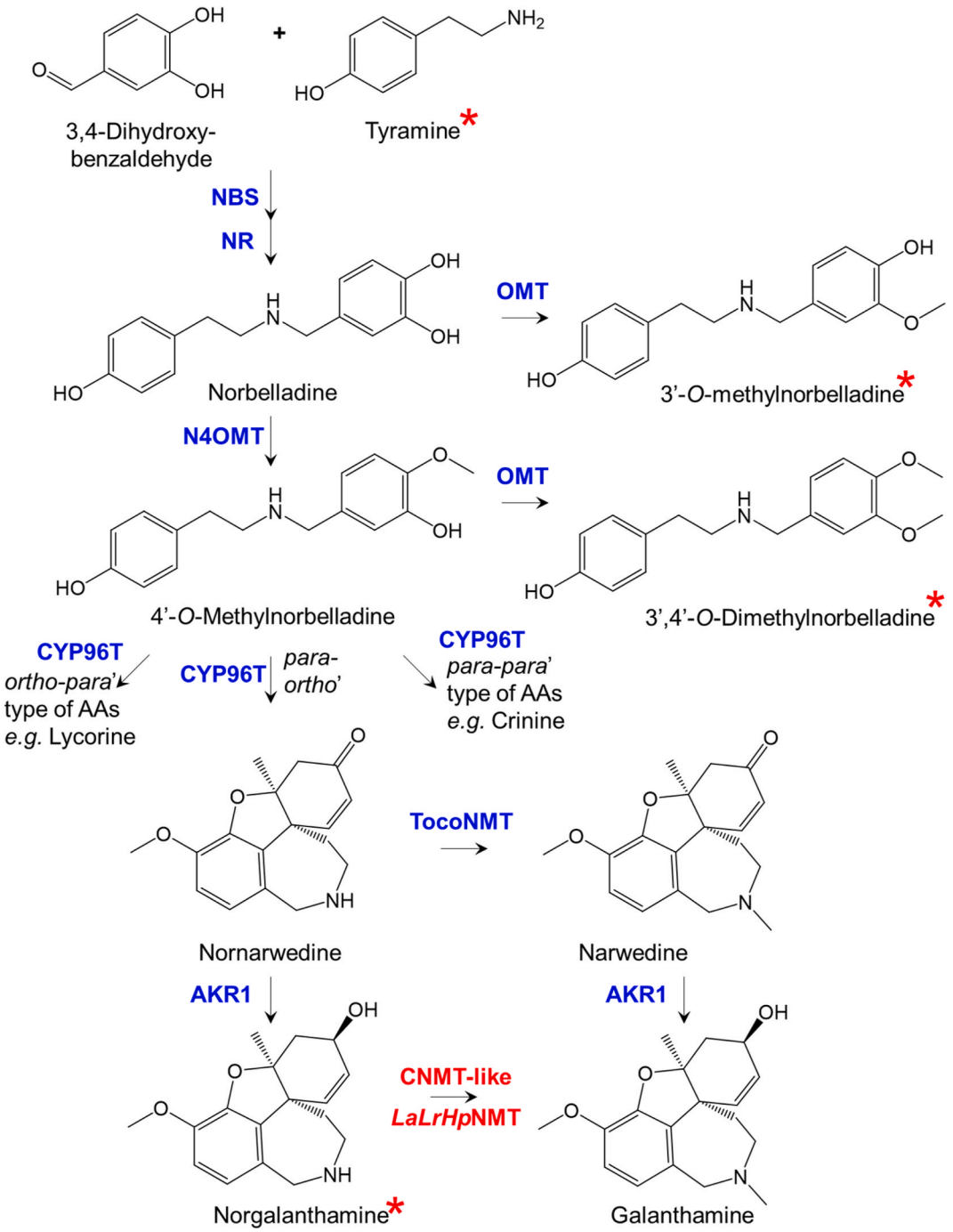

Fig. 1. Biosynthetic pathway leading to galanthamine starting from the condensation of tyramine and 3,4-DHBA. All enzymes shown in bold blue have been identified from Amaryllidaceae. Abbreviations are NBS, norbelladine synthase; NR, noroxomaritidine/norcraugsodine reductase; OMT, *O*-methyltransferase; N4OMT, norbelladine 4′-*O*-methyltransferase; CYP96T, cytochrome P450 monooxygenase 96T; TocoNMT, tocopherol *N*-methyltransferase; AKR1, Aldoketoreductase1; and CNMT-like *LaLrHp*NMT, coclaurine *N*-methyltransferase-like enzymes (five isoforms) from this study. * represents the substrates accepted by *LaLrHp*NMT1 characterized in this study. (For interpretation of the references to colour in this figure legend, the reader is referred to the Web version of this article.)

galanthamine *in planta* (Eichhorn et al., 1998; Jayawardena et al., 2024). Given the necessity for various *N*-methylation steps in AA biosynthesis (Desgagné-Penix, 2021), additional *N*-methyltransferases likely contribute to these pathways.

N-methyltransferases (NMTs) are enzymes that transfer a methyl group (-CH_3) to specified nitrogen atoms in substrates, typically using *S*-adenosylmethionine (SAM) as the methyl donor, resulting in the formation of *N*-methylated products (Zhou et al., 2020). This methylation process is crucial for altering and diversifying plant-specialized metabolites, such as alkaloids, by changing their solubility, stability, and biological activity, which can influence endogenous functions and therapeutic potential (Lee et al., 2024). For example, galanthamine exhibits strong anti-acetylcholinesterase inhibitory activity, whereas its demethylated form, norgalanthamine, a bit less (Orhan et al., 2021). In benzylisoquinoline alkaloid (BIA) biosynthesis, a subclass of isoquinoline alkaloids, multiple NMTs have been identified, including coclaurine-*N*-methyltransferases (CNMT), reticuline *N*-methyltransferases (RNMT), and tetrahydroxyprotoberberine *N*-methyltransferases (TNMT), each catalyzing specific methylation reactions critical for BIA structural diversity (Lee et al., 2024; Morris and Facchini, 2019).

In this study, we identified, isolated, and characterized CNMT-like NMTs from two commercially galanthamine-producing species, *L. aestivum* and *L. radiata*, and a high galanthamine-producing species, *Hippeastrum papilio*. We compared *CNMT-like NMT* expression levels and galanthamine content across different organs of these three species during the vegetative stage. Additionally, we investigated the subcellular localization of CNMT-like NMTs and analyzed how various stress conditions affect their expression. This study uncovers a new enzyme of the AA pathway and provides new insights into the regulation of *N*-methylation in AA biosynthesis, offering potential strategies for metabolic engineering to enhance galanthamine production.

2. Materials and methods

2.1. Plant materials and growth conditions

Mature bulbs of *L. aestivum* and *H. papilio* were purchased from Florissa (https://florissa.com), and *L. radiata* mature bulbs were bought from a plant nursery in China. Bulbs were planted in plastic pots in autoclaved soil (ARGO MIX G6 potting soil), grown at room temperature with 14 h:10 h light:dark condition for 12 months, watered weekly, and fertilized when necessary. Leaves, bulbs, and roots were separated when the plants were in the vegetative stage, flash-frozen in liquid nitrogen, and stored at −80 °C.

In vitro H. papilio shoot cultures were prepared for the stress treatment experiment as follows. After four weeks at 4 °C, a mature bulb of *H. papilio* was left at room temperature overnight. After a 1-h heat treatment at 52 °C, it was left to rest at room temperature for the night. Then, dead and dried scales were removed before sterilizing the bulb's surface. The bulb was then rinsed with tap water and detergent five times and submerged in 70 % ethanol for 1 min. After that, the bulb was exposed to commercial bleach that contained 6 % sodium hypochlorite for 30 min. The bulb was then repeatedly washed in a biological hood using autoclaved water five times. Finally, 2–3 mm size twin-scale explants were obtained with sterilized scalpels and forceps. Murashige and Skoog media supplemented with 3 % sucrose, 0.075 % plant preservative mixture, 3 $g.L^{-1}$ of Phytagel, and 15 μM benzyl aminopurine (BAP) were used as the basic shoot induction media. Before adding Phytagel and autoclaving, the pH was adjusted to 5.7 ± 0.1. Ten explants were cultivated in each plate under dark conditions at 25 °C. Every two weeks, the transplants were subcultured until the shoots appeared and grew to a length of a few centimeters to separate them. The shoots were then separated and cultivated in glass jars with the same media, with 5 μM BAP and 5 μM naphthalene acetic acid (NAA) at 25 °C under light conditions (14 h:10 h light:dark, 100 $\mu Mol.m^{2\ -1}$). Cultures were maintained for six months until sufficient material was produced. Then, shoots were transferred into 250 mL flasks containing liquid Murashige and Skoog media supplemented with 3 % sucrose, 0.075 % plant preservative mixture, 5 μM BAP, and 5 μm NAA, as ten shoots per flask, and maintained with the same growth chamber conditions for another two weeks. They were then treated for 0, 6, 24, and 48 h with 100 μM MeJA, 1 μM coronatine, 400 mM NaCl, 20 % PEG-6000 solution (w/v), 500 μM sodium nitroprusside (SNP), or 50 μM $CdCl_2$, individually. Shoot cultures were kept in chambers at 4 °C and 35 °C for 0, 6, 24, and 48 h to simulate cold and heat stress. The shoots were then collected, crushed with liquid nitrogen, and stored at −80 °C. The experiment was conducted in three replicates.

2.2. Chemicals and reagents

Standards of the alkaloids 11-hydroxyvittatine, 9-*O*-demethylhomolycorine, cherylline, flexinine, gigancrinine, gigantelline, gigantellinine, haemanthamine, homolycorine, obliquine, pancracine, sanguinine, tazzetine, vittatine and crinine were kindly obtained from Professor Antonio Evidente (Institute of Biomolecular Chemistry, National Research Council, Pozzuoli, NA, Italy). Standards of 3′-*O*-methylnorbelladine, 4′-*O*-methylnorbelladine, 3′,4′-*O*-dimethylnorbelladine, and norbelladine were synthesized as described in (Girard et al., 2022). Standards of 3,4-dihydroxybenzaldehyde (97 %), 4-hydroxybenzaldehyde (99 %), isovanillic acid (99 %), isovanillin (98 %) and trans-cinnamic acid (98 %) were purchased from Acros Organics (Massachusetts, USA). Standards of 3,4-dihydroxybenzoic acid (97 %), levodopa (98 %), L-tyrosine (99 %), and *p*-coumaric acid (98 %) were purchased from Alfa Aesar (Massachusetts, USA). Standards of caffeic acid (98 %), dopamine (98 %), ferulic acid (99 %), lycorine (98 %), papaverine (98 %), tyramine (99 %), and vanillin (99 %) were procured from Millipore Sigma (Massachusetts, USA). Standards of galanthamine (98 %) and narciclasine (98 %) were purchased from Tocris Bioscience (Bristol, United Kingdom). Standards of norgalanthamine, lycoramine (97 %), coclaurine (95 %), isoferulic acid (98 %), and phenylalanine (98 %) were obtained from Toronto Research Chemicals (Ontario, Canada), US Biological, Musechem (New Jersey, USA), TCI America (Oregon, USA), and MP Biomedicals (California, USA) respectively. Analytical LC-MS grade methanol was purchased from Fisher Scientific (New Hampshire, USA).

2.3. Identification of NMT transcripts

In the assembled transcriptome of *Leucojum aestivum*, one complete transcript was annotated as CNMT-like NMT(Tousignant et al., 2022). The exact transcript was blasted against the laboratory's in-house transcriptome database containing publicly available Amaryllidoideae transcriptomes, already assembled or assembled using Trinity 2.14.0 with default parameters (Lamichhane et al., 2025), to identify the candidates from *L. radiata* and *Hippeastrum* cv. hybridum using blast+ 2.130. Primers for restriction cloning and qRT-PCR were prepared using those sequences (Supplementary Table A1), and for the qRT-PCR, a universal primer pair was used (Supplementary Table A2).

2.4. Quantitative real-time expression of NMT

Total RNA was extracted from three different organs (leaves, roots, and bulbs) of the three selected species (*L.* aestivum, *L. radiata*, and *H. papilio*) using the GeneJET Plant RNA Purification Kit (Thermo Scientific™) and from the stress-treated shoot cultures of *H. papilio* using TRIzol reagent (Invitrogen), according to the manufacturer's instructions, using 100 mg of flash-frozen homogenized tissues. A NanoPhotometer (Implen) and 1.5 % (w/v) agarose gel electrophoresis were used to confirm the amount and quality of RNA isolated from various tissues. cDNA was synthesized from 1 μg of the freshly extracted RNA using SuperScript™ IV VILO™ Master Mix (Invitrogen™) according to the product manual. After that, RT-qPCR was carried out using 1 μL of

cDNA and 0.25 mM of gene-specific primers (Supplementary Table A2) in Luna Universal qPCR Master Mix (New England Biolabs) to assess the expression of two genes: *histone 3*, as an endogenous reference gene, and *NMT*, which codes for *N*-methyltransferase. The $2^{-\Delta Ct}$ method was used to calculate the gene's relative expression. The results obtained were analyzed and visualized using GraphPad Prism 10 software.

2.5. Extraction, LC-MS detection, and quantification of Amaryllidaceae alkaloids

One hundred milligrams of the homogenized fresh tissues and 20 mg of lyophilized shoot cultures of *H. papilio* were utilized to extract metabolites. One milliliter of 90 % methanol was added to extract the crude metabolites, left in the sonication bath for 1 h and then in a water bath at 60 °C for 2 h. After that, 0.2 μm PTFE syringe filters were used to filter the extracts. The SpeedVac Vacuum Concentrator (Thermo Fisher) evaporated the solvents completely. After being weighed and reconstituted in the mobile phase (methanol and milli-Q water (90:10), both containing formic acid 0.1 % v/v) as 1000 mg.L^{-1} of crude plant metabolite extract, with 1 mg.L^{-1} papaverine as an internal standard, the dry crude extract was again filtered through 0.2 μm PTFE syringe filters.

A high-performance liquid chromatography (HPLC) coupled with a tandem mass spectrometer (MS/MS) (Agilent, QC, Canada) equipped with an Agilent Jet Stream ionization source, a Kinetex EVO C18 column (150 × 4.6 mm, 5 μm, 100 Å; Phenomenex, Torrance, USA), a binary pump, an autosampler set at 4 °C and a column compartment were used for the analysis. Five microliters of each sample were injected into the column set at 30 °C. A gradient made of (A) formic acid 0.1 % v/v in Milli-Q water and (B) formic acid 0.1 % v/v in methanol, with a flow rate of 0.4 mL/min, was used to achieve chromatographic separation. The HPLC elution program started with 10 % solvent B; 0–10 min, isocratic conditions with 10 % solvent B; 10–20 min, linear gradient to reach 100 % B; 20–25 min, isocratic conditions with 100 % B; 25–26 min, linear gradient to return to initial conditions of 10 % B. The total run time was 30 min per sample to allow the reconditioning of the column before the next injection. The parameters used for the MS/MS source to perform the analyses were set as follows: gas flow rate 10 L/min, gas temperature 300 °C, nebulizer 45 psi, sheath gas flow 11 L/min, sheath gas temperature 300 °C, capillary voltage 4000 V in ESI$^+$ and 3500 V in ESI$^-$ and nozzle voltage 500 V. Agilent MassHunter Data Acquisition (version 1.2) software was used to control the HPLC-MS/MS, MassHunter Qualitative Analysis (version 10.0) and MassHunter Quantitative QQQ Analysis (version 10.0) software were used for data processing. Multiple reaction monitoring (MRM) transitions and instrument parameters used for targeted compound identification during HPLC-MS/MS analysis are included in Supplementary Tables A3 and A4. A standard calibration curve was prepared as follows: a working stock solution containing galanthamine at 100 mg mL^{-1} in LC-MS grade methanol. This stock solution was further diluted to prepare calibration solutions with the following concentrations in triplicate: 0, 1.25, 2.5, 5, 50, 1000, 2000, 5000, and 10000 ng mL^{-1}, to which the internal standard papaverine was added at a final concentration of 1000 ng mL^{-1} each. These standard solutions were injected into the HPLC-MS/MS system to generate calibration curve regression. Supplementary Fig. A1 shows the calibration curve obtained by plotting the area ratio (*i.e., the* peak area of galanthamine divided by the peak area of the papaverine) as a function of galanthamine's concentration, which allowed galanthamine quantification in the various tissues of *L.* aestivum, *L. radiata*, and *H. papilio*. The results obtained were analyzed and visualized using GraphPad Prism 10 software.

2.6. Isolation, cloning, and heterologous protein production

The open reading frames of CNMT-like NMTs from the three different Amaryllidoidae species (*L.* aestivum, *L. radiata*, and *H. papilio*) were amplified using the leaf cDNA using Terra™ PCR mix (Takara Bio) in 50 μl with 0.3 μM of gene-specific primers having EcoRI and HindIII restriction sites (Supplementary Table A2) according to the user manual. A typical PCR cycle consisted of 98 °C for 2 min, followed by 98 °C for 10 s, 60 °C for 15 s, 68 °C for 1.5 min for 40 cycles, followed by 5 min hold at 68 °C and then an infinite hold at 4 °C. After digestion, the amplified cDNA region was cleaned using high-fidelity EcoRI and HindIII restriction enzymes (New England Biolabs) with the Geneaid GenepHlow Gel/PCR kit. The digested PCR products were cloned into pMAL-c2X vectors using T4 DNA ligase (New England Biolabs) in frame with maltose-binding protein (MBP). Heat shock was used to transform the recombinant plasmids into chemically competent *E. coli* DH5α cells, and colonies were chosen on LB agar plates supplemented with ampicillin (100 mg mL^{-1}, Thermo Fisher Scientific). The presence of the targeted gene was verified by colony PCR, and the identity of the gene was confirmed by sequencing (three clones per transformation) using Sanger sequencing at the Genome Quebec sequencing facility.

2.7. NMT sequence analysis and phylogenetics

The NMT clones from this study and their corresponding sequences are available in Supplementary Table A5. Protein molecular weights and pI predictions were made using the Expasy tool (Supplementary Table A6) (https://www.expasy.org/resources/compute-pi-mw/). The candidate NMTs studied here were aligned to the amino acid sequences of the characterized NMTs in the BIA alkaloid pathway (obtained from NCBI, https://www.ncbi.nlm.nih.gov, Table 1) using the Clustal Omega algorithm integrated with Unipro UGene version 46.0 (Okonechnikov et al., 2012). Phylogenetic analysis was done using the aligned sequences by PhyML maximum likelihood method with LG substitution model with 1000 bootstraps employed in Unipro UGene version 46.0 (Okonechnikov et al., 2012).

2.8. In silico analysis of NMT

Folding prediction of coclaurine-like *N*-methyltransferase candidates and mutants from *L. aestivum*, *H. papilio,* and *L. radiata* was performed using AlphaFold Server Beta powered by AlphaFold3 (Abramson et al., 2024). Receptor preparation and docking were performed using the MOE2022.09 software with the AMBER10:EHT force field (Chemical Computing Group) performed the reactor preparation and docking. Predicted enzymes were superimposed with reference crystal structures of *Cj*NMT in MOE (6GKY (Bennett et al., 2018b)). Methyl donor *S*-adenosylmethionine (SAM) was included in the active sites at coordinates of orthologous crystal structures (see Supplementary Fig. A2). The docking site was predicted based on residues in interaction with ligands of orthologous crystal structure and included SAM. Ligands (norgalanthamine, tyramine) isomeric smiles codes retrieved from PubChem were

Table 1
List of *N*-methyltransferases used for alignment and phylogenetic tree in this study. Sequences were obtained from NCBI (https://www.ncbi.nlm.nih.gov).

Species	Name	Accession number
Aristolochia fimbriata	*Af*CNMT	ADP76529.1
Coptis japonica	*Cj*CNMT	BAB71802.1
Ephedra sinica	EsNMT	AWJ64115.1
Eschscholzia californica	*Ec*TNMT	ACO90222.1
Liriodendron chinense	*Lc*CNMT1	Lchi24863
Nelumbo nucifera	*Nn*CNMT	WEE66564.1
Papaver somniferum	*Ps*CNMT	Q7XB08.1
Papaver somniferum	*Ps*RNMT	AOR51552.1
Papaver somniferum	*Ps*TNMT	AAY79177.1
Thalitricum flavum subsp. glaucum	*Tf*CNMT	Q5C9L6.1
Thalitricum flavum	*Tf*PavNMT	ACO90251.1
Stephania intermedia	*Si*CNMT1	QFU85193.1
Stephania intermedia	*Si*CNMT2	QFU85194.1
Sinopodophylum hexandrum	*Sh*CNMT	AJD20224.1

submitted to the ZINC20 database to obtain 3D charged data files (Irwin et al., 2020). Protomers predicted at pH = 8.5 were included as possible ligands.

Triangle Matcher was selected as a placement method for 200 poses generated by flexible docking with tethered induced fit refinement. Ten docking poses for each ligand were compared with crystalized protein-ligand complexes. The pose with the best docking score coherent with the catalyzed reaction was selected. PLIP was used to detect the interactions between ligands and receptor residues (Adasme et al., 2021). Visualization, superimposition, and figure preparation were performed using Pymol 3.0.0 (Schrödinger).

2.9. NMT site-directed mutagenesis and cloning

Ten *LaLrHp*NMT1 mutant constructs were generated by Gibson assembly using the NEBuilder® HiFi DNA Assembly Bundle for Large Fragments (New England Biolabs, Canada). Fragments for the assemblies were amplified by PCR with PrimeSTAR GXL DNA Polymerase (Takara Bio, Japan) according to the manufacturer's protocol, using the plasmid pMAL-c2X_*LaLrHp*NMT1 as the template and the primers listed in Table A2 in Supplementary Data. *E. coli* DH5α cells were transformed, and mutagenesis was confirmed, as described in section 2.6. Heterologous protein production and enzymatic assays. Purified recombinant plasmids were transformed into chemically competent *E. coli* Rosetta (DE3) pLysS (Novagen) by heat shock for heterologous enzyme production. Colony PCR was conducted to screen positive transformants, and then protein expression and purification were done. Seed cultures were prepared for protein production with 12.5 mL of LB medium supplemented with 100 μg mL^{-1} ampicillin and 35 μg mL^{-1} chloramphenicol using single colonies incubated overnight at 37 °C with orbital shaking at 200 rpm. The following day 250 mL of LB media in 1 L flasks (containing 100 μg mL^{-1} of ampicillin and 35 μg mL^{-1} of chloramphenicol) were inoculated with the seed cultures and incubated in the same conditions for a few hours until reaching the OD of the cultures to $A_{600} = 0.6$; after cooling on ice, IPTG was added to the cultures at a final concentration of 1 mM to induce the generation of recombinant protein, they had been cultivated at 18 °C with orbital shaking at 200 rpm for 16 h. Cells were extracted by centrifugation at 5000*g* for 10 min at 4 °C. After that, the cell pellets were stored at −80 °C until protein purification. Enzyme purification was initiated by re-suspending the cells in 25 mL of protein extraction buffer (30 mM Tris–HCl, pH 8, 150 mM NaCl, 1 mM EDTA, 10 % (v/v) glycerol). They were then incubated for 30 min on ice and sonicated for 8 min (15 s on, 30 s off). The crude lysate was centrifuged at 16,000 g for 15 min at 4 °C to eliminate cellular debris. One milliliter of amylose resin beads (New England Biolabs) was added to the cleared supernatant and then incubated at 4 °C while constantly shaken. The mixture was run through a gravity column at 4 °C after an hour, and the remaining beads were then rinsed three times using the same buffer without NaCl. Elution buffer, the same as lysis buffer without NaCl but containing 25 mM of freshly made maltose, was used to elute the purified enzymes. Using bovine serum albumin as the standard, the Bradford reagent was used to measure the concentration of purified MBP-tagged protein utilizing the manufacturer's procedure (Thermo Fisher Scientific). Protein purity was evaluated using a 10 % (w/v) SDS-PAGE gel. Freshly purified enzymes were utilized for enzymatic tests.

After that, the recombinant NMTs' enzymatic activity for the synthesis of galanthamine was evaluated. A 50 μL mixture of 50 mM Tris-HCl (pH 8.5), 500 μM SAM as the methyl donor, 250 μM norgalanthamine as the substrate, and 50 μg of pure protein was used to conduct the reaction. Purified MBP-tag protein from the empty vector was used as the negative control. After 16 h of incubation at 37 °C, the mixtures were terminated by adding 50 μL of methanol. Following 15 min of centrifugation at 10,000 rpm at 4 °C, adding papaverine at 20 $mg.L^{-1}$ as internal standard and performing a sample dilution of 20-fold in the mobile phase (methanol and milli-Q water (90:10), both containing formic acid 0.1 % v/v), LC-MS/MS analysis was carried out.

Instrumentation and chromatographic conditions for enzyme assays done with norgalanthamine as substrate were conducted as described in subsection 2.5, except that the only compounds monitored by the LC-MS/MS during those enzymatic assays were norgalanthamine, galanthamine, and papaverine.

2.10. Optimization of enzymatic conditions

Since *LaLrHp*NMT1 was present in all three species and had the maximum activity for galanthamine synthesis, it was used to determine optimal parameters, kinetics, and substrate specificity. Tests were conducted for 16 h under the same circumstances as the initial enzymatic tests in 50 mM Tris-HCl, pH 8.0, and between 10 and 70 °C to identify the ideal temperature. Next, assays were conducted in 50 mM sodium phosphate buffer (pH 6.0–7.0), Tris-HCl (pH 7.0–9.0), and glycine/NaOH buffer (pH 9.0–10.0) at 42 °C for 16 h to identify the ideal pH.

2.11. Substrate specificity assay

Next, substrate specificity was determined by incubating 250 μM of possible substrates for 16 h at 42 °C in 50 mM Tris-HCl, pH 8.5, to determine the substrate specificity. The chemical structure of these substrates is presented in Supplementary Fig. A3. Purified protein denatured by boiling for 10 min was used in adverse control reactions. After 16 h of incubation at 37 °C, the mixtures were terminated by adding 50 μL of methanol. Following 15 min of centrifugation at 10,000 rpm at 4 °C, adding papaverine at 20 $mg.L^{-1}$ as internal standard and performing a sample dilution of 20-fold in the mobile phase (methanol and milli-Q water (90:10), both containing formic acid 0.1 % v/v), LC-MS/MS analysis was carried out. The same LC-MS/MS methodology described in subsection 2.5 was applied to analyze samples from substrate specificity assays, except that they were analyzed in Single Ion Monitoring (SIM) mode instead of MRM. Each substrate was monitored by the mass-to-charge (m/z) ratio corresponding to their molecular weight ionized in positive electrospray ionization (ESI^+) (*i.e.* $[M+H]^+$).

In contrast, the corresponding expected product was monitored with an added mass of +14 m/z, +28 m/z, and/or +42 m/z (*i.e.* $[M + H+14]^+$, $[M + H+28]^+$ and/or $[M + H+42]^+$) to determine if one, two or three N-methylation reaction(s) occurred on the substrate during assays. Analyses were done using authentic standards to obtain the retention time of each substrate and by comparing Extracted Ion Chromatograms (EIC) from assays to the ones of corresponding negative controls. New signals detected at the expected retention time and m/z of the product(s) or a more abundant signal compared to negative controls were considered positive results for those experiments. Each assay, along with negative controls, was performed in triplicate. Supplementary Table A3 presents the instrumental parameters used for analyzing substrate specificity tests by LC-MS/MS. The substrate conversion percentage was calculated based on the decrease in substrate levels in the enzymatic assay compared to the negative control relative to the formation of the added mass of +14 m/z, +28 m/z, and/or +42 m/z.

2.12. In vivo enzymatic assay and subcellular localization in planta

The *LaLrHp*NMT1 gene from *Leucojum aestivum* was amplified from cDNA using Takara high-fidelity DNA polymerase in a 25 μL reaction volume. The PCR mixture consisted of 12.5 μL of enzyme, 1.5 μL of each primer (10 mM), 1 μL of template cDNA, and 8.5 μL of distilled water. Amplification was carried out with an initial denaturation at 98 °C for 30 s, followed by 30 cycles of denaturation at 98 °C for 10 s, annealing at 72 °C for 30 s, and extension at 72 °C for 1.3 min, concluding with a final extension at 72 °C for 5 min. The AttB-flanked PCR products were purified using the Gel/PCR DNA Fragment Purification Kit (Geneaid) and subjected to a Gateway BP recombination reaction with the pDONR221 vector (Thermo Fisher Scientific). The resulting entry clone was

transformed into *Escherichia coli* DH5α, and positive clones were selected on LB agar containing 50 μg mL^{-1} kanamycin. Sequence identity was verified by sequencing, and the clones were further used in LR recombination reactions with pK7WG2 for *in vivo* assay, and either the pB7FWG2 (*C*-terminal GFP) or pB7WGF2 (*N*-terminal GFP) destination vectors for localization experiment. Positive *E. coli* DH5α transformants were selected on LB agar containing 50 μg mL^{-1} spectinomycin.

The *LaLrHp*NMT1 constructs in pK7WG2, pB7FWG2, or pB7WGF2 were then introduced into *Agrobacterium tumefaciens* strain GV3101 via electroporation, and positive colonies were selected on LB agar plates containing rifampicin, spectinomycin, and gentamicin (50 μg mL^{-1} each) at 28 °C. Single colonies were cultured in LB media supplemented with the appropriate antibiotics, harvested, and washed twice with induction buffer (10 mM $MgCl_2$, 10 mM MES, pH 5.6, 200 μM acetosyringone). The cultures were adjusted to an OD_{600} of 0.6 and incubated in induction buffer for 2 h at room temperature. These *A. tumefaciens* cultures harboring the gene of interest were infiltrated into 4-week-old *Nicotiana benthamiana* leaves. In the *in vivo* assay, norgalanthamine (100 μM) was infiltrated 48 h later, and plants were further incubated for 24 h. Leaves were harvested, and metabolite analysis was performed by LC-MS/MS as in (Lamichhane et al., 2025). For co-localization analysis, pB7FWG2 or pB7WGF2 constructs were co-infiltrated with RFP (nucleo-cytosolic marker) and mCherry (ER marker with a signal peptide). Forty-eight hours post-infiltration, abaxial epidermal cells were imaged using a Leica TCS SP8 confocal laser scanning microscope with a 40x oil immersion objective. GFP fluorescence was excited at 488 nm with emission detected between 500 and 525 nm, chlorophyll autofluorescence was excited at 552 nm with emissions detected between 620 and 670 nm, and mCherry fluorescence was excited at 587 nm with emission detected at 619 nm. Image processing was performed using the Leica LasX software.

3. Results

3.1. Candidate coclaurine-like NMT mining, expression analysis, and galanthamine levels in tissues of three species of Amaryllidaceae

The coclaurine-like NMT candidate was identified by searching annotated transcripts in the transcriptome of *L. aestivum* (Tousignant et al., 2022). A single, complete mRNA sequence (1065 bp) encoding a 355 amino acid protein was detected and selected as the *CNMT-like NMT* candidate for this study. This sequence served as a query to BLAST against our Amaryllidoideae transcriptome database (Lamichhane et al., 2025), identifying one ortholog in both *L. radiata* and *Hippeastrum* cv. hybridum transcriptomes. We designed a universal RT-qPCR primer pair for gene expression analysis targeting conserved regions across all three *CNMT-like NMT* sequences. In contrast, species-specific primers were developed for cloning into expression vectors (Supplementary Table A2).

CNMT-like NMT expression levels varied among tissues (leaf, bulb, and root) of the three species, with the highest expression observed in leaves of *H. papilio* at 2.65 ± 0.87, over twice that of the other species (Fig. 2A). In contrast, *L. aestivum* roots exhibited the lowest *NMT* expression level, recorded at 0.03 ± 0.03, while *L. radiata* showed moderate expression across all sampled organs (Fig. 2A). Galanthamine accumulation patterns did not mirror exactly these expression trends (Fib. 2B). Bulbs of *H. papilio* contained especially high galanthamine concentrations, reaching 1.62 ± 0.07 mg per gram of fresh tissue. In contrast, galanthamine levels were relatively moderate in *L. aestivum* tissues and lowest in *L. radiata,* where it was only detected in bulbs and not in the leaves and roots (Fig. 2B).

3.2. Amaryllidaceae NMT candidates cluster together with coclaurine NMTs

After verifying NMT transcripts' expression in galanthamine-producing plants, full-length transcripts were cloned and analyzed. In L. *aestivum*, three isoforms were identified: *LaNMT1* identical to the reference mRNA sequence, *LaNMT2* with two nucleotide differences; and *LaNMT3,* which contained 19 substitutions (Supplementary Table A5). In L. *radiata*, two isoforms were detected: *LrNMT1,* which displayed 42 nucleotide substitutions compared to the reference *NMT* sequence, and four silent nucleotide differences relative to *LaNMT1*, and *LrNMT2*, which exhibited 38 substitutions compared to the reference sequence. *H. papilio* presented two unique sequences: *HpNMT1*, identical to the reference sequence, and *HpNMT2*, which contained 13 nucleotide substitutions (Supplementary Table A5). *LaNMT1, LrNMT1*, and *HpNMT1* encoded an identical amino acid sequence, which we designated *LaLrHpNMT1*. Thus, five unique isoforms from three species were included in this study. All sequences were 1068 bp long and translated into a protein of 355 amino acids. *LaLrHp*NMT1, *La*NMT2, *La*NMT3, *Lr*NMT2, and *Hp*NMT2 displayed theoretical molecular weights of 41.3,

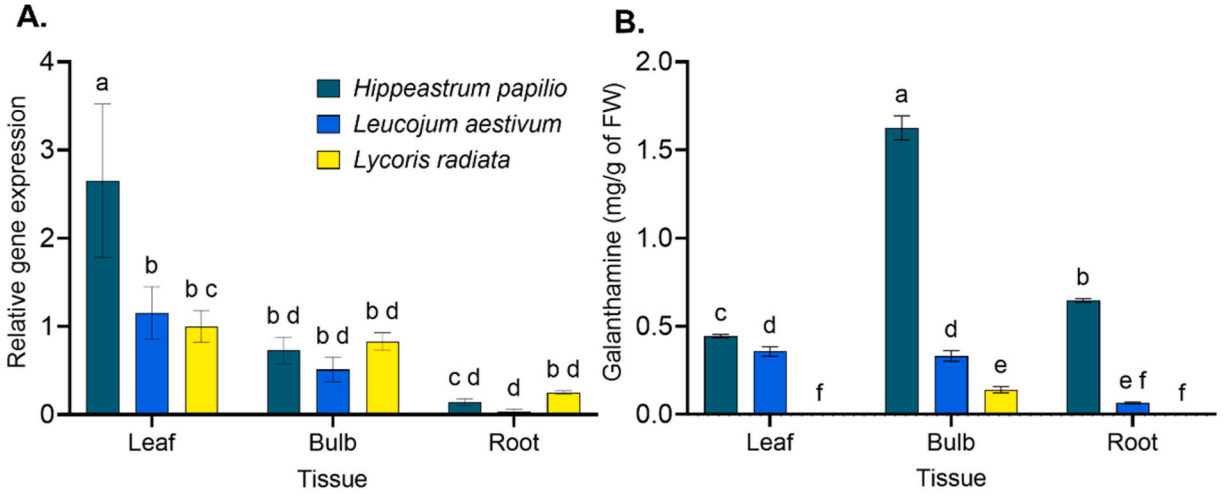

Fig. 2. Comparison of relative expression of NMT with galanthamine content of three Amaryllidaceae in different tissues in the vegetative stage. **A.** Relative NMT expression ($2^{-(\Delta\Delta Ct)}$) was measured by qRT-PCR normalized by the housekeeping gene Am_Histone3. **B.** Galanthamine content was measured by LC-MS/MS using authentic standard and a standard curve. All the values are shown as means ± standard deviation of three independent biological replicates. Plants were grown under the same conditions for 12 months before the experiment. Statistical significance was calculated with a two-way ANOVA followed by Tukey's multiple comparisons. Lowercase letters indicate significant differences between treatments ($p < 0.05$).

41.2, 41.3, 41.3, and 41.3 kDa and isoelectric points of 6.09, 6.09, 6.56, 6.76, and 8.48, respectively (Supplementary Table A6). The predicted isoelectric points are similar for all the enzymes except *Hp*NMT2.

Phylogenetic analysis showed that the five Amaryllidaceae NMT isoforms form a distinct clade with *Nn*CNMT (*Nelumbo nucifera*) and *Si*CNMT1 (*Stephania intermedia*), suggesting evolutionary conservation (Fig. 3A). This clade was closely related to *phenylalkylamide EsNMT* from *Ephedra sinica*, forming a distinct subgroup. *Si*CNMT2 from *S. intermedia* was positioned adjacent to this cluster, suggesting possible functional and structural similarities among these enzymes. In contrast, a separate clade included CNMTs from *Thalictrum flavum* subsp. *glaucum*, *Liriodendron chinense*, *Sinopodophyllum hexandrum*, *Aristolochia fimbriata*, and *Coptis japonica*. A more distant phylogenetic relationship was observed between the candidates and *reticuline NMT* (RNMT) or *tetrahydroxyprotoberberine NMT* (TNMT), consistent with previous studies (Liscombe, Usera, and O'Connor, 2010).

At the amino-acid level, the five Amaryllidaceae NMT isoforms exhibited high similarity (91–99 %), supporting a close evolutionary relationship and a potential functional conservation. These isoforms shared 40–80 % similarity with known NMTs involved in BIA biosynthesis (Supplementary Table A7), aligning with previously observed evolutionary patterns in BIA pathways (Morris and Facchini, 2019; Morris et al., 2018; Cheng et al., 2022). Additionally, the isoform sequences exhibited approximately 62 % similarity with

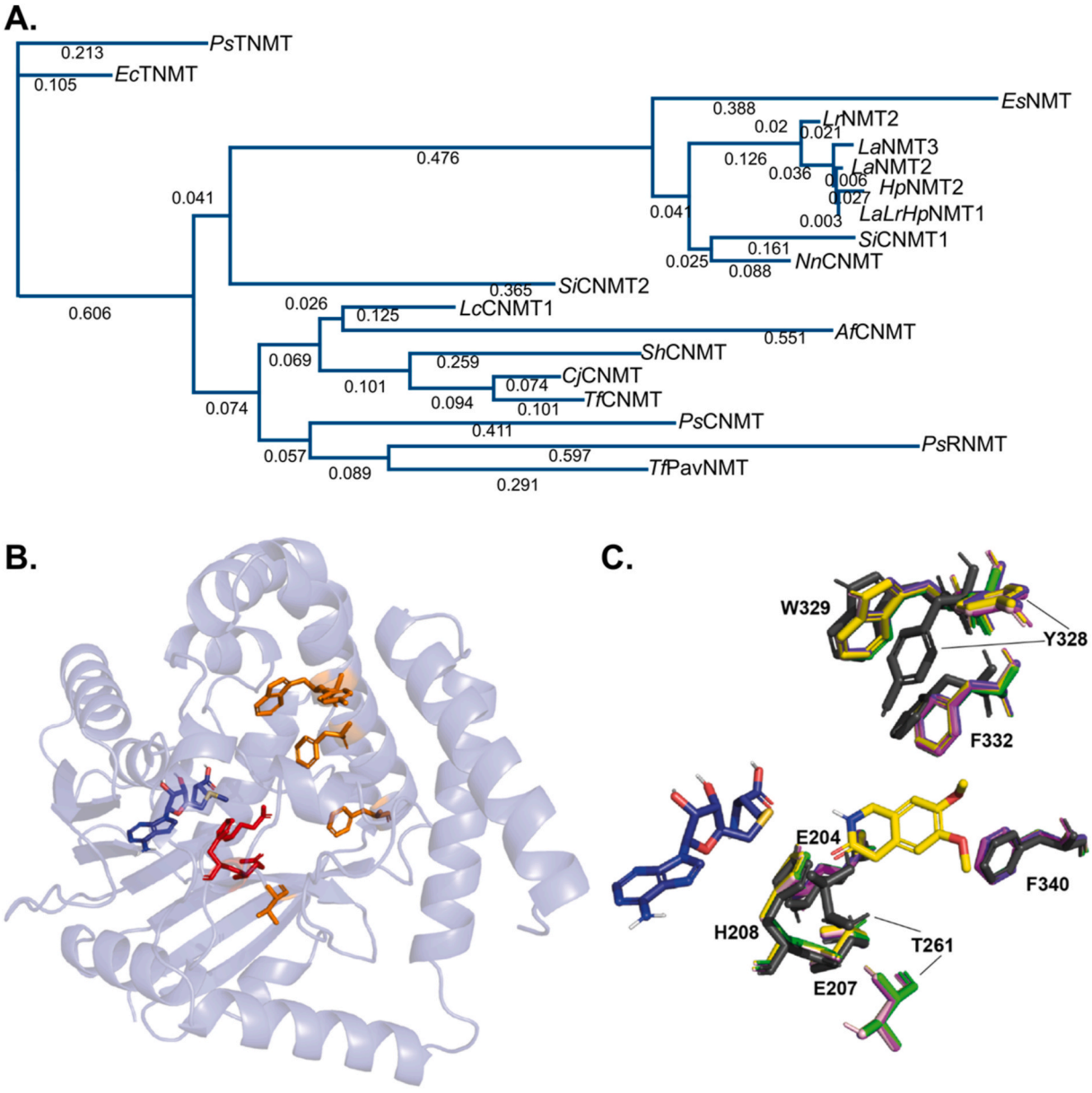

Fig. 3. *In silico* analysis of coclaurine-like NMT candidates from *Leucojum aestivum*, *Hippeastrum papilio*, and *Lycoris radiata*. **A.** The evolutionary relationships of the NMTs in this work and other identified plant NMTs from the BIA alkaloid pathway are compared using a phylogenetic tree. The aligned sequences were used for the phylogenetic analysis using the PhyML maximum likelihood technique with the LG substitution model and 1000 bootstraps used in Unipro UGene version 46.0. The National Centre for Biotechnology Information (NCBI) search engine (http://www.ncbi.nlm.nih.gov/protein/) was used to get the amino acid sequences of the plant BIA NMT. The methodology includes the accession numbers. **B.** AlphaFold3 predicted the folding of *LaLrHp*NMT1 in cartoon representation, with putative catalytic residues (Glu204, Glu207, and His208) as red sticks and other conserved active site residues as orange sticks. SAM is shown as purple sticks. **C.** Superimposed conserved active site residues of Amaryllidaceae CNMT-like enzyme candidates with *Cj*NMT pocket (dark grey sticks) containing SAM (dark purple sticks) and heliamine (yellow sticks). *La*NMT2 is shown in yellow, *La*NMT3 light pink, *Lr*NMT2 bright pink, *LaLrHp*NMT1 violet, and *Hp*NMT2 green. Residues are numbered according to the *Cj*NMT structure. (For interpretation of the references to colour in this figure legend, the reader is referred to the Web version of this article.)

phenylalkylamide *Es*NMT, indicating possible evolutionary divergence. *Cj*CNMT and *Si*CNMT showed 75 %–82 % similarity with the Amaryllidaceae NMT isoforms, coinciding with the phylogenetic analysis (Fig. 3A–Supplementary Table A7).

3.3. Conserved catalytic residues and active site conformation

The predicted structures of the CNMT-like enzyme candidates were compared to the *Cj*NMT crystal structure (Fig. 3B). The Amaryllidaceae NMT isoforms exhibited high structural similarity, with root mean square deviation (RMSD) values ranging from 0.105 to 0.146 Å and were closely aligned with the *Cj*CNMT folding pattern (RMSD = 0.515 Å) (Fig. 3B). This overall structure followed the class I methyltransferase α/β Rossmann fold and a catalytic pocket composed mainly of α-helices (Fig. 3B). Superimposition with *Cj*CNMT showed a high degree of structural conservation, except for the *N*-terminal α-helices, which were predicted with lower confidence by AlphaFold3 (Fig. 3B).

The Amaryllidaceae NMT isoforms shared conserved regions with other NMT enzymes involved in BIA biosynthesis (Fig. 3B and C, Supplementary Fig. A2 and A4). All five isoform sequences exhibited typical SAM-dependent methyltransferase domain, which is critical for catalytic activity and is characteristic of BIA-pathway NMTs (Morris and Facchini, 2019). They shared catalytic residues Glu207 and His208 with RNMTs and TNMTs (Morris et al., 2020), and Glu204 with CNMTs, replacing Gly204 in RNMTs and Ala204 in pavine NMTs (PavNMTs) (Morris et al., 2020). Glu204, Glu207, and His208, as well as active site residues Trp329, Phe332, and Phe340 shared a similar orientation across all isoforms, remaining close to the SAM methyl group and the substrate in CNMTs (Fig. 3C, Supplementary Fig. A2), where they are implicated in stabilizing ligand interactions via H-bonding or salt-bridge formation (Bennett et al., 2018a). Glu204 and His208 act as a catalytic dyad, while Glu207 plays a key role in PavNMT catalysis. During *N*-methylation of coclaurine by *Cj*CNMT, Glu204 stabilizes the H-N bond of the substrate to pull the electron and yield protonated nitrogen. Site-directed mutagenesis showed that His208 functions as a general base, deprotonating the substrate's ammonium ion to enable a nucleophilic attack on the methyl group of SAM (Bennett et al., 2018a).

Several other key catalytic residues were conserved across the studied NMTs and known CNMT enzymes, including Thr261, Phe340 (Phe337 in Amaryllidaceae), Tyr328 (Tyr325 in Amaryllidaceae), Trp329 (Trp326 in Amaryllidaceae), and Phe332 (Phe329 in Amaryllidaceae) (Bennett et al., 2018a). Thr261, Tyr325 (or Ser325 in *HpNMT2*), and Phe329, were arranged differently from the reference CNMT crystal structure (Fig. 3C). In CNMTs, Tyr328, Trp329, and Phe332 are particularly important for substrate binding and orientation relative to SAM, as demonstrated by the loss of activity following their mutation, although the effect is less pronounced for Tyr328 (Bennett et al., 2018a). Interestingly, a serine residue is observed in *HpNMT2 at this position*, suggesting a potential functional variation in this isoform (Supplementary Fig. A2 and A4).

3.4. CNMT-like Amaryllidaceae NMTs catalyze N-methylation of norgalanthamine to produce galanthamine

To investigate if Amaryllidaceae NMT isoforms were involved in galanthamine formation (Fig. 4A), we assessed whether norgalanthamine could fit within the putative enzyme active site pocket in a position conducive to *N*-methylation. We performed flexible docking simulations using *LaLrHp*NMT1 as the receptor. The predictions revealed conserved interactions with catalytic residues Glu204 (forming an H-bond with the ligand nitrogen) and His208 (forming an H-bond with the oxygen), with a score of −7.9 kCal.mol^{-1} (Fig. 4B–Supplementary Table A8). However, interactions with Tyr325, Phe329, and Phe337 were not predicted. Instead, an alternative H-bond with Tyr288 (with the nitrogen of norgalanthamine) and hydrophobic interactions with Phe234 and Phe257, which stabilized its rings, were observed. These results suggest a conserved mechanism of action for this CNMT-like enzyme, supporting norgalanthamine as a viable substrate. Furthermore, the involvement of alternative residues hints at a possible substrate promiscuity, allowing the enzyme to accommodate various structurally related alkaloid substrates.

To validate this prediction, we evaluated the *in vitro* catalytic activity of the five heterologously produced Amaryllidaceae NMT isoforms for their ability to catalyze galanthamine synthesis from norgalanthamine, as determined by LC-MS/MS analysis (Fig. 4C). All tested NMT isoforms exhibited detectable activity above background levels (compared to the negative control, Fig. 4C). Specifically, *LaLrHp*NMT1 (79.93-fold compared to control) and *Hp*NMT2 (69.38-fold) produced significantly higher amounts of galanthamine compared to the other three enzymes ($p < 0.0001$, One-way ANOVA). In contrast, *La*NMT3 exhibited the lowest activity (11.7-fold, $p = 0.9998$) (Fig. 4C). Despite a 99 % similarity between *La*NMT2 and *LaLrHp*NMT1 (differing by only three amino acid differences: Pro68Leu, Asn151Tyr, and Leu234Phe), the activity of *La*NMT2 was significantly lower (30.32-fold, $p = 0.0004$, one-way ANOVA), suggesting that these specific residues play a crucial role in enzymatic efficiency (Fig. 3, Supplementary Table A7, Fig. 4C). Notably, *Hp*NMT2 exhibited similar catalytic efficiency to *LaLrHp*NMT1, despite containing a serine at position 325 instead of a tyrosine, indicating functional tolerance for this substitution with the enzyme active site. The optimal enzymatic parameters were evaluated for *LaLrHp*NMT1, the most active isoform, by assessing its activity across a pH range from 6.0 to 10.0 and a temperature range of 10–70 °C. The enzyme exhibited peak activity *in vitro* at pH 8.5 and 42 °C (Fig. 4D and E). To substantiate the enzyme's functionality, we conducted *in vivo* assays by expressing *LaLrHp*NMT1 in *Nicotiana benthamiana* leaves, infiltrating norgalanthamine as substrate (Fig. 4F). A significant level of galanthamine ($p < 0.05$) was observed in *N. benthamiana* leaves in two out of three plants. These results showed that *LaLrHp*NMT1 catalyzes norgalanthamine *N*-methylation *in vitro* and *in vivo*.

3.5. Mutational analysis reveals essential residues for LaLrHpNMT1 activity

Docking analysis suggested that norgalanthamine interacted with several key active site residues. Among them, Glu204, Phe234, and Phe257 were selected as mutation site candidates to enhance the catalytic efficiency of *LaLrHp*NMT1 for *N*-methylation of norgalanthamine. These residues were mutated into amino acids with similar (Phe234Leu/Ala/Trp, Phe257Leu/Ala/Trp, Glu204Asp) or distinct physicochemical properties (Glu204Lys/Gln). Docking simulations were performed to evaluate the potential effects of these mutations on substrate binding. Most mutations did not result in a noticeable change in the binding energy of norgalanthamine within the enzyme pocket, except for two mutations, *i.e.,* Phe257Ala and Glu204Gln, which exhibited a binding energy difference of >1 kcal/mol and an increased distance between SAM and the substrate (Supplementary Table A9). Consequently, these two mutants were excluded as candidates for enhancing enzyme activity. Interaction with catalytic residue His208 was conserved for all mutants except Phe257Ala and Phe257Leu. Similarly, interactions with Glu204 were conserved in Phe mutants, except for Phe257Ala. Mutations of Glu204 led to a conserved interaction with the ligand for Lys204 or Asp204, but not Gln204. The latter resulted in norgalanthamine forming new H-bonds with His80 and Tyr98. Glu204Asp lost hydrophobic bonding with Val333, whereas in Glu204Lys, norgalanthamine lost interactions with Phe234 but won Phe329. In Glu204Gln, a new bond with Phe337 was predicted. Hydrophobic interaction with Phe329 was observed in all Phe257 mutants and Phe234Leu, while new interaction with Phe337 was predicted for Phe234Ala. Structurally, Phe337 is positioned near Phe234, whereas Phe329 is adjacent to Phe257 in the enzyme active site. Interestingly, the Phe234Trp mutation was predicted to disrupt interactions between the substrate and the active site Phe residues, suggesting that mutations at this position could alter enzyme

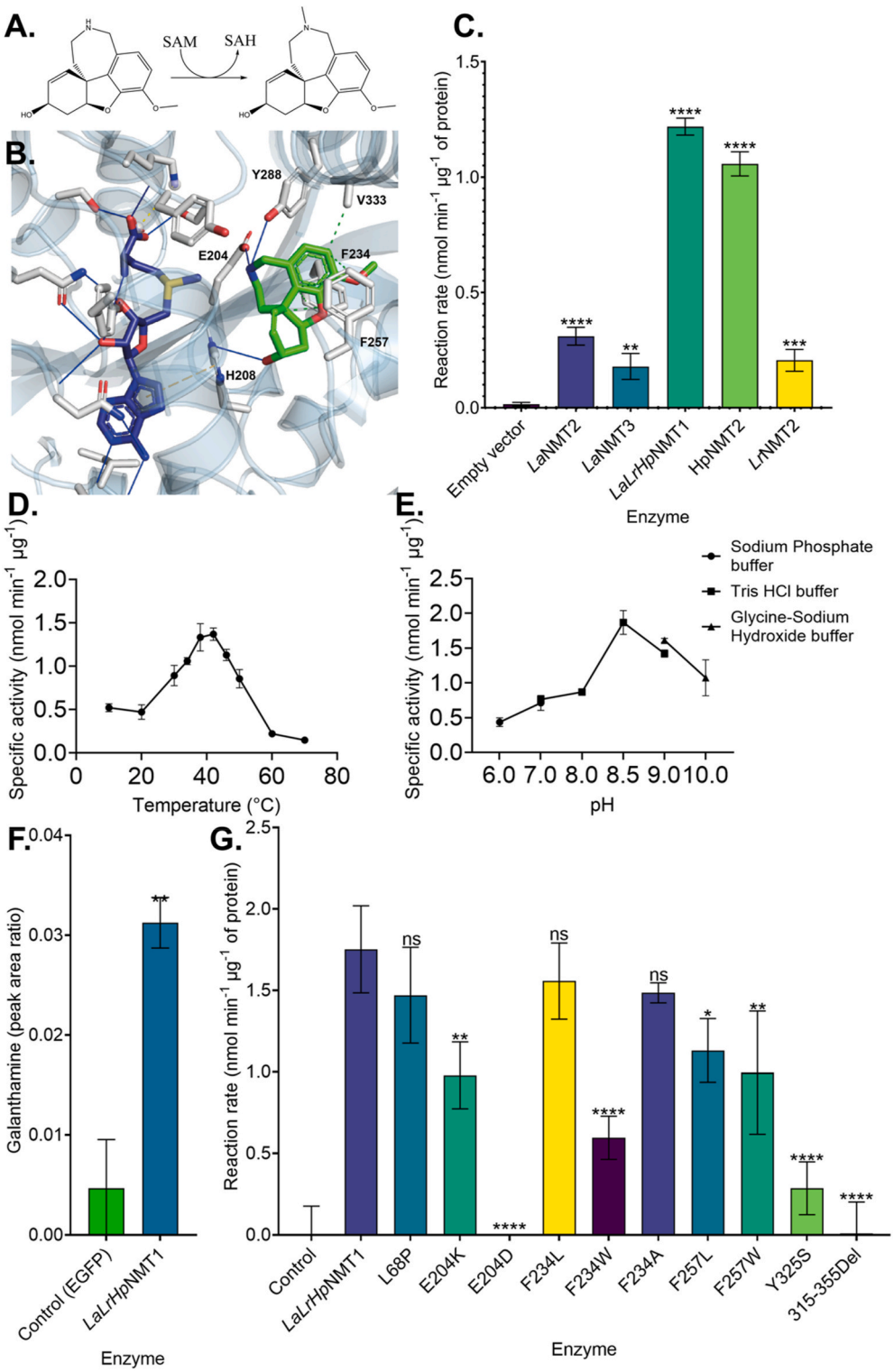

Fig. 4. Amaryllidaceae coclaurine-like N-methyltransferases catalyze N-methylation of norgalanthamine. **A.** Schematic conversion of norgalanthamine to galanthamine. **B.** *LaHpLr*NMT1 active site residue (grey) in interaction with docked norgalanthamine (green) and SAM (dark purple). H-bonds are shown as blue lines, p-stacking interaction as yellow dashed lines, and hydrophobic interactions as green dashed lines. **C.** Comparison of the activity of the five heterologously produced Amaryllidaceae NMT isoforms for the catalysis of norgalanthamine to galanthamine. Control: the empty vector was used here as the negative control. **D.** Production rate of galanthamine for *LaLrHp*NMT1. under different pH. **E.** Production rate of galanthamine for *LaLrHp*NMT1 under different temperatures. **F.** Relative quantification of galanthamine *in planta*. The area ratio was obtained by dividing the peak area of galanthamine by the internal standard papaverine. *N. benthamiana* infiltrated with *Agrobacterium* harboring EGFP, which was used as a negative control. Three biological replicates were included, and galanthamine was detected in two out of three samples. The bar *LaLrHp*NMT1 represents the mean of the two positive samples with standard deviation. **G.** Comparison of the activity of the mutants of *LaLrHp*NMT1 for the production of galanthamine. Data are shown as means ± SD of three biological repeats with background subtracted. *p* values presented as Dunnett's multiple comparisons test of one-way ANOVA. **** = $p < 0.0001$, *** = $p < 0.001$, ** = $p < 0.01$. (For interpretation of the references to colour in this figure legend, the reader is referred to the Web version of this article.)

activity.

To assess the functional impact of these mutations, enzyme activity was evaluated based on the ability of *LaLrHp*NMT1 variants to yield galanthamine (Fig. 4G). In addition to the active site mutations tested by docking; two more substitutions were introduced to explore their potential impact on enzyme function. Tyr325Ser was selected because *Hp*NMT2 naturally possesses Ser325, whereas all four other homologs contain Tyr325. Similarly, Leu68 is conserved in *LaLrHp*NMT1 and *Hp*NMT2, while the other three isoforms carry a Pro at this position. A truncated version of the enzyme was generated by removing residues 315–355 to evaluate the importance of the C-terminal region in catalysis. None of the mutations resulted in an increase in norgalanthamine N-methylation. The Glu204Asp mutant and the truncated enzyme variant (315–355Δ) exhibited a complete loss of activity ($p < 0.0001$). Phe234Trp ($p < 0.0001$) and Tyr325Ser ($p < 0.0001$) mutants resulted in a significant reduction in galanthamine production. Glu204Lys ($p = 0.0022$), Phe257Leu ($p = 0.0159$), and Phe257Trp ($p = 0.0027$) retained lower but detectable levels of activity. Leu68Pro, Phe234Leu, and Phe234Ala did not result in a significant modulation of galanthamine production. These findings suggest that Glu204, Phe234, and Tyr325 play critical roles in enzyme function.

3.6. *LaLrHpNMT1 is promiscuous*

To investigate the substrate promiscuity of the CNMT-like enzyme *LaLrHp*NMT1, we tested its ability to convert 18 different substrates possessing free hydrogen on the nitrogen (Supplementary Fig. A3), making them potential candidates for *N*-methylation. Methylation activity was confirmed by detecting both a decrease in substrate concentration and the appearance of a new signal in ESI^+ mode with a mass-to-charge ratio (m/z) corresponding to the molecular weight of the expected methylated product ($[M + H+14]^+$). The tested substrates included aromatic amino acids (phenylalanine, tryptophan and tyrosine), amines (tryptamine, tyramine, *N*-methyltyramine, hordenine), AAs (norgalanthamine, norbelladine, 3′-*O*-methylnorbelladine, 3′,4′-*O*-dimethylnorbelladine, 4′-*O*-dimethylnorbelladine) and *N*-demethylated plant alkaloids (huperzine, heliamine, coclaurine, *N*-demethylricinie) (Supplementary Fig. A3).

*LaLrHp*NMT1 demonstrated *N*-methylation activity on eight substrates: heliamine (42.23 %), huperzine A (28.76 %), norgalanthamine (25.11 %), tryptamine (25.03 %), tyramine (24.09 % converted), 3′,4′-*O*-dimethylnorbelladine (15.84 %), 3′-*O*-methylnorbelladine (8.64 %), *N*-desmethylivabradine (2.49 %) (Fig. 5). Among them, heliamine, a basic tetrahydroisoquinoline structure, was most efficiently converted substrate, consistent with its known role as a preferred substrate of CNMTs (Bennett et al., 2018a). While *LaLrHp*NMT1 did not methylate aromatic amino acids, it accepted their decarboxylated amines, tryptamine and tyramine, at levels comparable to norgalanthamine (~25 %). Interestingly, despite clustering phylogenetically with CNMT enzymes (Fig. 3A), *LaLrHp*NMT1 did not accept coclaurine as a substrate. It catalyzed the *N*-methylation of 3′-*O*-methylnorbelladine and 3′,4′-*O*-dimethylnorbelladine but not of norbelladine or 4′-*O*-methylnorbelladine (Fig. 5), suggesting that methylation at 3′-*O* position may be required for *in vitro* enzyme activity.

3.7. *LaLrHpNMT1 localizes in the cell cytoplasm, and ER*

Key enzymes involved in the AA biosynthetic pathway in *L. aestivum*—*La*NBS, *La*NR, and *La*N4′OMT—are localized in the cytosol, while *La*CYP96T is associated with the endoplasmic reticulum (ER) (Desgagne-Penix et al., 2024; Majhi et al., 2023). To determine the subcellular localization of *LaLrHp*NMT1, we expressed both N- and C-terminal enhanced green fluorescent protein (eGFP)-tagged constructs and assessed their distribution in plant cells (Fig. 6). The integrity of the fusion proteins was confirmed via Western blot (Supplementary Fig. A5). Fluorescence microscopy revealed similar localization between the two constructs (Fig. 6). Both the N- and C-terminally tagged *LaLrHp*NMT1 constructs displayed strong fluorescence signals in the cytosol as well as the ER (Fig. 6), indicating a dual site localization pattern.

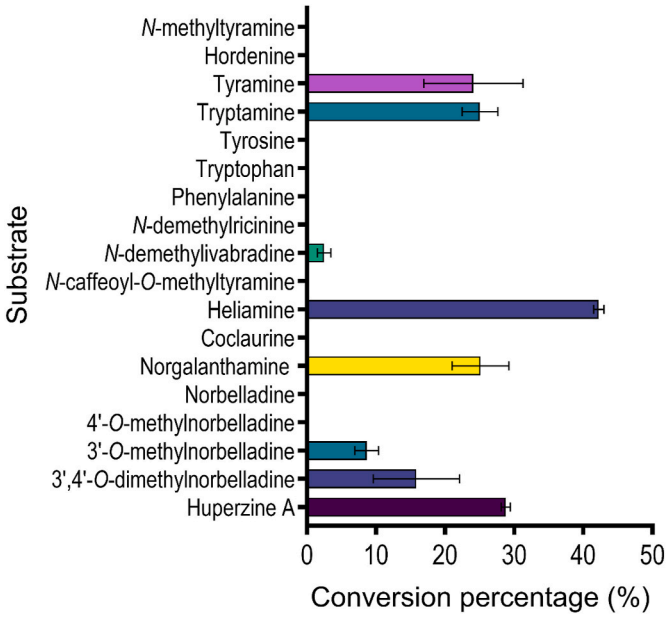

Fig. 5. Substrate specificity of *LaLrHp*NMT1 tested with multiple demethylated substrates. *N*-methylation catalysis was considered significant when both a decrease in substrate amount and detection of a signal with m/z corresponding to the molecular weight of the expected product ionized in ESI^+ with an added mass of +14 m/z ($[M + H+14]^+$) were considered. The conversion percentage was calculated as the decrease in substrate compared to the negative control, i.e., heat-deactivated enzyme. Values are presented as mean ± SD with three independent replicates.

3.8. *Up-regulation of NMT expression under different environmental stresses*

The current supply of galanthamine primarily depends on plant extraction (Berkov et al., 2022). *In vitro,* shoot culture has been extensively studied as a more sustainable and cost-effective means of producing AAs (Berkov et al., 2022; Ptak et al. 2016, 2020; Koirala et al., 2022), and it is well established that environmental stresses can act as potent inducers of alkaloid biosynthesis (Ali et al., 2019; Koirala et al., 2023). In this study, we examined the effects of different environmental stressors on *H. papilio* shoot cultures by evaluating relative gene expression levels of NMT and alkaloid production at 6, 24, and 48 h post-treatment (Fig. 7, Supplementary Figure A8-15). Chemical stress inducers included methyl jasmonate (MeJA), the bacterial toxin coronatine, $CdCl_2$, saline (NaCl), and sodium nitroprusside (SNP). Physical stressors included cold (4 °C), heat (35 °C), and drought (PEG6000).

Intriguingly, *NMT* expression responded to all tested stress conditions, with a 1.2- to 6.4-fold increase in expression compared to controls (Fig. 7). Heat stress had the most pronounced and sustained effect, with a mean relative gene expression of 6.464 ± 1.179. Other stressors, such as coronatine, $CdCl_2$, saline, cold, and drought, triggered a sharp increase in *NMT* levels within the first 6–24 h, followed by a gradual decline, though expression remained significantly elevated compared to untreated controls. For example, MeJA treatment resulted in a 1.345 ± 0.12 increase in relative *NMT* expression after 6 h, which rose to 3.132 ± 0.403 at 24 h before decreasing to 2.048 ± 0.271 at 48 h (Fig. 7).

Concomitant targeted metabolite analysis revealed that galanthamine accumulation varied under different stress conditions (Supplementary Fig. A8–A16), especially after adding MeJA,

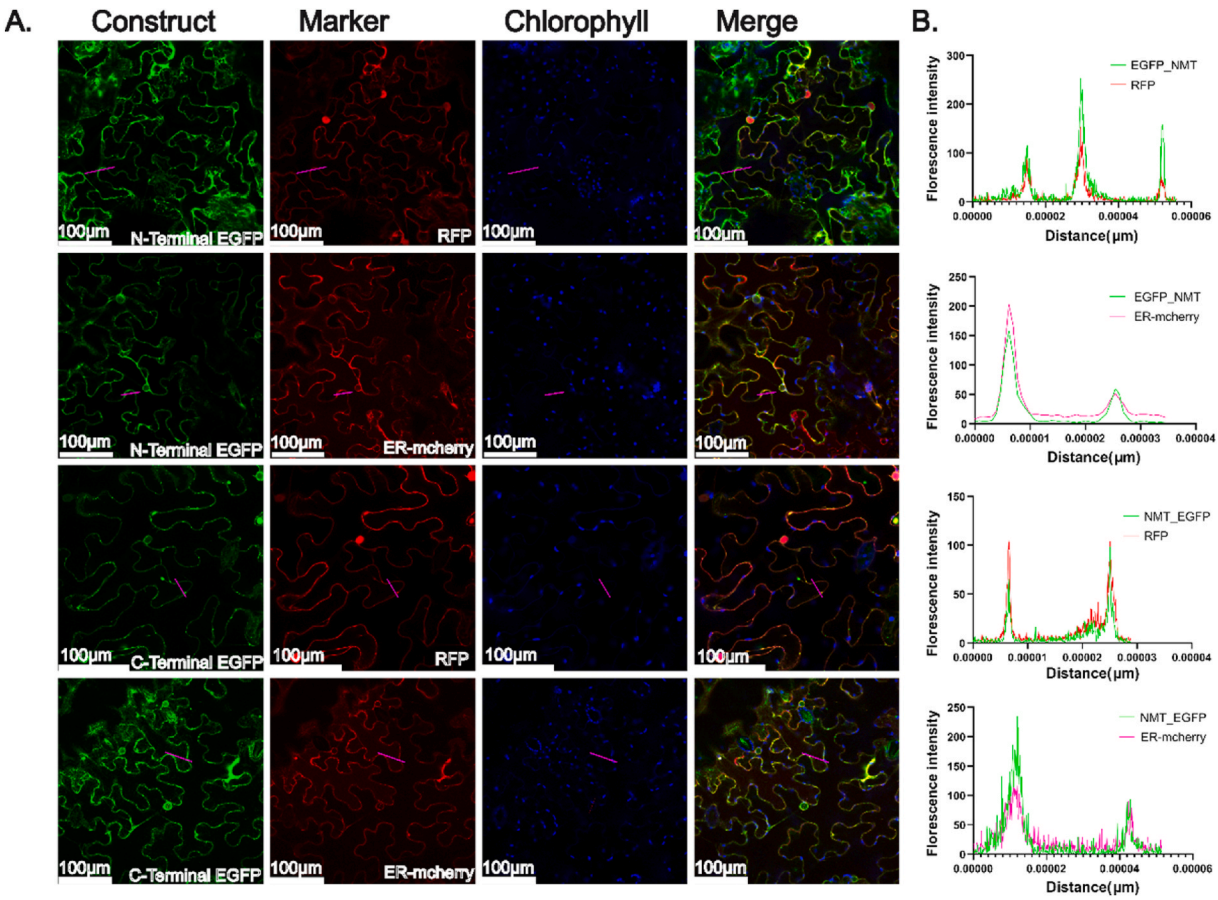

Fig. 6. *LaLrHp*NMT1 localizes in the cytoplasm and endoplasmic reticulum. **A.** Subcellular localization of eGFP-tagged NMT. N- and C-terminal GFP fusion *LaLrHp*NMT1 was co-expressed with red fluorescent protein (RFP) or ER-mCherry constructs in the epidermal cell of *Nicotiana benthamiana* leaves, and images were taken after 48 h with confocal microscopy. Panels 1 and 3 display *LaLrHp*NMT1-eGFP with RFP, whereas Panels 2 and 4 show *LaLrHp*NMT1-eGFP with ER-mCherry. For all panels, chlorophyll and merge images, along with **B.** fluorescent intensity during co-localization, are shown in the graph. The scale bar represents 100 μm. (For interpretation of the references to colour in this figure legend, the reader is referred to the Web version of this article.)

coronatine, heat, and $CdCl_2$. There was no positive correlation between levels of galanthamine and *NMT* gene expression (Pearson r = −0.02368, $p = 0.9048$). Nonetheless, there was a positive correlation with narwedine (Pearson r = 0.3823, $p = 0.0447$), 11-hydroxyvittatine (Pearson r = 0.5326, $p = 0.0035$) and crinine/vittatine (Pearson r = 0.5256, $p = 0.0041$) (Supplementary Table A9). These correlations further support the involvement of NMT in the AA biosynthetic pathway.

4. Discussion

The present study focused on the functional characterization of CNMT-like NMT in Amaryllidaceae. First, to investigate a potential link between *CNMT-like NMT* expression and galanthamine biosynthesis, we measured transcript expression and alkaloid levels in different tissues of three Amaryllidoideae species. *H. papilio* displayed the highest quantities of galanthamine across all tissues (Fig. 2B), aligning with previous studies highlighting this species as a rich source (Berkov et al., 2022). Although *this species* displayed the highest levels of *NMT* expression as well, the two factors, *i.e.,* galanthamine and transcript levels, were not correlated regarding their repartition across tissues. *NMT* was expressed across tissues of *L. radiata*, but galanthamine was undetectable in the leaves and roots (Fig. 2), suggesting that its accumulation may be highly species- and tissue-specific.

A recent study proposed that young leaves are the preferential site of AA biosynthesis in Amaryllidaceae, a result consistent with the higher expression of our candidates in the three here-studied species (Mehta et al., 2024). However, other studies comparing gene expression of other key enzymes implicated in the early AA pathway, such as NBS, NR, and OMT in *L. aestivum* and *L. radiata,* have indicated that the biosynthetic origin of AA is not clear, and transcripts levels do not necessarily correlate with enrichment in AA. For example, relative gene expression of *NBS* is higher in roots, while *NR* and *OMT* transcript levels are enriched in bulbs of *L. aestivum* and *L. radiata* at the flowering stage, and galanthamine accumulates more in the bulbs (Majhi et al., 2023; Li et al., 2019; Karimzadegan et al., 2024). During the vegetative stage of *N. papyraceus, OMT* and *NR* expression were higher in bulbs, and *NBS* was enriched in roots that contained more AAs (Koirala et al., 2024). These differences imply that AAs' biosynthetic pathways and accumulation sites may vary significantly by environment, species, tissue type, and growth stage. The blooming season may also impact gene expression, suggesting that AA biosynthesis is complex and not restricted to a uniform tissue-specific pattern across different species. These findings indicate that galanthamine accumulation is not solely determined by the transcript expression of AA biosynthetic enzymes, such as *NMT*, and that additional factors, such as enzyme activity, substrate availability, transport mechanisms, or regulatory pathways, may influence its distribution across tissues.

Among the identified isoforms, *LaNMT1, LrNMT1*, and *HpNMT1* encoded an identical protein sequence, suggesting strong conservation across species. The theoretical molecular weights of all five isoforms identified in this study were consistent with previously characterized CNMT-like NMTs, such as *Si*CNMT1 and *Si*CNMT2 from *Stephania intermedia* and *Nn*CNMT from *Nelumbo nucifera* (Zhao et al., 2020; Chen

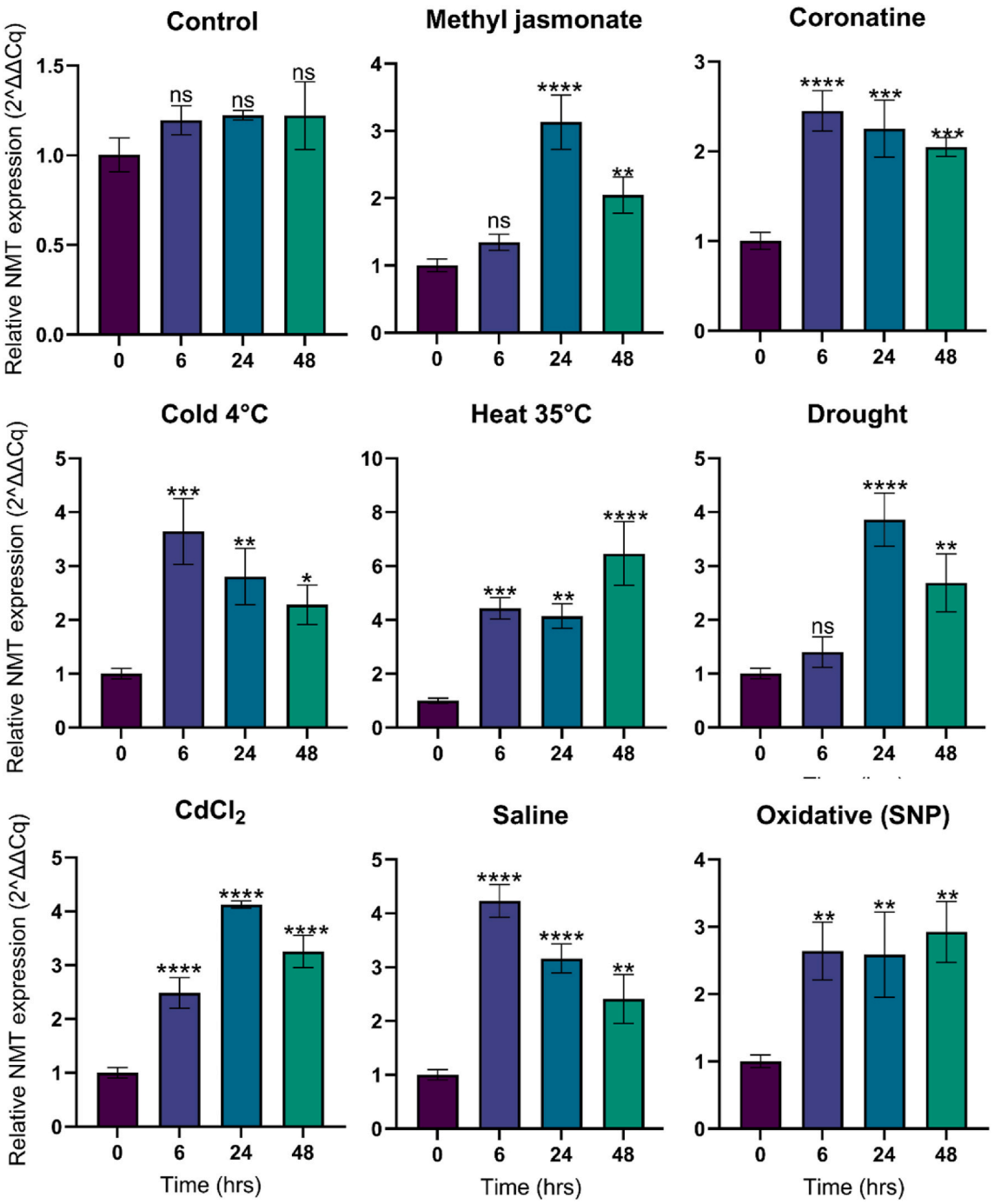

Fig. 7. Relative expression patterns of *NMT* following stress treatments of *H. papilio* shoot cultures. Shoots liquid cultures were treated with different stresses: methyl jasmonate, coronatine, cold (4 °C), heat (35 °C), drought (20 % PEG6000), $CdCl_2$, saline (NaCl), and sodium nitroprusside (SNP) for oxidative stress, for 48 h. RT-qPCR measured relative *NMT* expression with samples collected at 6-, 24-, and 48-h intervals and normalized to the housekeeping gene *Am_Histone3*. The *NMT* expression of the control at 0 h was taken as the relative expression 1.00 ($2^{-(\Delta\Delta Ct)}$); the values are shown as means ± standard deviation of three independent biological replicates. All the *in vitro* shoots were derived from a single *H. papilio* bulb and grown for 6 months before the experiment. Dunnett's multiple comparisons test of one-way ANOVA was used to assess statistical significance. **** = $p < 0.0001$, *** = $p < 0.001$, ** = $p < 0.01$, * = $p < 0.1$, ns = p values are not significant.

et al., 2024), indicating a conserved structural profile. However, the predicted isoelectric points were generally similar, except *HpNMT2*, which displayed a notably higher pI, potentially reflecting differences in biochemical properties or stability.

The phylogenetic clustering patterns of CNMTs from *N. nucifera* and *S. intermedia* with target Amaryllidaceae NMTs, along with their proximity to the phenylalkylamide NMT from *E. sinica* (Fig. 3), suggests a conserved evolutionary trajectory likely linked to structural requirements for methylation in isoquinoline-based molecules (Morris et al., 2018; Chen et al., 2024; Zhao et al., 2020; Rønsted et al., 2012). Amaryllidaceae NMTs may have evolved from a common ancestral NMT, which later diverged to facilitate specialized alkaloid biosynthetic pathways, including AA and BIA. In contrast, the divergence of CNMTs from *T. flavum*, *L. chinense*, *S. hexandrum*, *A. fimbriata*, and *C. japonica* into a separate clade may indicate functional specialization or lineage-specific adaptations within their plant families (Cheng et al., 2022). This phylogenetic distance aligns with the hypothesis that evolutionary pressures have driven substrate specificity and catalytic

function diversification, particularly in pathways involving coclaurine or similar intermediates in alkaloid biosynthesis. The clustering of *phenylalkylamide EsNMT* within the same group suggests a shared methylation mechanism among species and potentially reflects convergent evolution in the biosynthesis of phenylalkylamide and isoquinoline (AA) alkaloids despite taxonomic divergence (Morris et al., 2018). The phylogenetic analysis *points to an earlier evolutionary split between gymnosperm and angiosperm NMTs, reinforcing* the idea that selective pressures across diverse plant lineages have driven the structural convergence of NMTs, optimizing their function in alkaloid biosynthesis.

The conservation of catalytic motifs across the Amaryllidaceae NMTs and BIA-pathway NMTs supports a shared evolutionary origin and suggests functional conservation in alkaloid biosynthesis. Glu204 and His208 as a catalytic dyad in CNMTs and their implication in substrate stabilization and methyl transfer indicate that similar enzymatic mechanisms may be at play in the studied candidates. The serine substitution at position 325 in *Hp*NMT2 could reflect a substrate specificity or enzyme activity divergence, possibly linked to species-specific adaptations in alkaloid metabolism. Overall, the sequence and structure analysis highlights the conservation of catalytic domains coclaurine-like NMTs from AA and BIA biosynthesis (Lee et al., 2024; Morris and Facchini, 2019). The structural folding analysis of the Amaryllidaceae NMT isoforms indicates that they could accommodate isoquinoline alkaloids as potential substrates for *N*-methylation, supporting the functional link between these enzyme families.

The *in vitro* assays confirmed that all five heterologously produced Amaryllidaceae NMT isoforms catalyze the *N*-methylation of norgalanthamine to galanthamine (Fig. 4), supporting their functional role in AA biosynthesis. *LaLrHp*NMT1 and *Hp*NMT2 were the most potent, yielding 4-5-fold more galanthamine than other isoforms. The most active isoform, *LaLrHp*NMT1, exhibited peak activity *in vitro* at pH 8.5 and 42 °C (Fig. 4). Its expression in *Nicotiana bethamiana* leaves confirmed its activity *in vivo*. CNMTs from BIA-producing plants, such as *N. nucifera* and *S. intermedia*, have been reported to function optimally with a basic pH range (7.5–9) and at temperatures between 35 and 45 °C *in vitro* (Chen et al., 2024; Zhao et al., 2020). Optimal activity conditions of NMTs may differ due to evolutionary adaptation to different biochemical environments and substrate specificities. These findings confirm that the putative NMT isoform identified in *H. papilio*, *L. aestivum,* and *L. radiata* catalyzes the *N*-methylation of norgalanthamine, a key step in galanthamine biosynthesis.

The variability in catalytic efficiency across the tested enzymes suggests that specific amino acid substitutions significantly influence enzymatic activity. Several mutations targeting Leu68, Glu204, Phe234, Phe257, and Tyr325 were introduced to understand the role of specific polymorphic residues or to confirm their role in the active site. In the active site, Phe234Trp mutation resulted in a loss of activity and hydrophobic interaction with the 234th residue and Phe257. By contrast, Phe234Leu conserved enzyme activity and interaction with Phe329 and the 234th mutated residue. Phe257Trp exhibited reduced activity despite conserving norgalanthamine interaction with Phe234 and gaining Phe329 hydrophobic bond. A previous study showed that Phe257Ala mutation in *Nn*CNMT increased the production of nuciferine more than two-fold (Chen et al., 2024). This particular mutation was not performed here as the docking simulation predicted >1 kCal/mol difference and an increased distance between SAM and norgalanthamine. This suggests that Phe234 and Phe257 are not essential for catalysis but could contribute to substrate orientation. The larger size of tryptophan might explain why it did not fully substitute for Phe at this position.

Despite the similar nucleophilic nature of Glu and Asp, Glu204Asp resulted in a complete loss in activity. The slight difference in pKa could lead to a subtle difference in enzyme activity at the pH used for the enzyme reaction (Herrington and Kellogg, 2021). The loss could also be caused by the difference in the size of the two amino acids. Glu204Lys, which maintained a similar nucleophilic property, resulted in a slight decrease in enzyme activity. Previous studies on CNMTs showed that flipping the amino acids from Glu204Gly and Gly204Glu resulted in a loss of catalysis of the canonical substrate (Morris et al., 2020).

Two additional residues were mutated, Leu68Pro and Tyr325Ser. Further from the ligand, Tyr325 was shown to be important for the reaction catalyzed by other CNMTs (corresponding to Tyr328)(Bennett et al., 2018a). Interestingly, *Hp*NMT2, which showed high galanthamine synthesis catalysis, contained instead for Ser325. Similarly, while *LaLrHp*NMT1 and *Hp*NMT2 displayed Leu at the 68th position, other isoforms, with less activity, encoded for a proline. Thus, we tested if the corresponding mutations would alter *LaLrHp*NMT1 activity. While Leu68Pro had no significant impact, Tyr325Ser resulted in a drastic decrease in *LaLrHp*NMT1 enzyme activity. This finding is consistent with a previous study (Bennett et al., 2018a), suggesting that mutating Ty325 impacts substrate positioning or active site conformation. However, the results also indicate that the required residue at this position is context-dependent, as *Hp*NMT2 with Ser325 had high activity. Overall, the results strengthen the evidence that Glu204, Phe234, Phe257, and Tyr325 play a key role in norgalanthamine *N*-methylation in the enzyme active site. While the role of His208 is well known (Bennett et al., 2018a), other key ligand interacting residues, such as Tyr288 and Val333, remain to be characterized.

Subcellular localization of NMTs varies across different biosynthetic pathways. For instance, the NMT involved in monoterpenoid indole alkaloid biosynthesis, which catalyzes the final step of vinblastine production, is chloroplastic (Dethier and De Luca, 1993). In contrast, CNMT and TNMT from *P. somniferum* (opium poppy) localized in the cytosol (Hagel and Facchini, 2012; Facchini and St-Pierre, 2005). The dual cytosolic and ER localization of *LaLrHp*NMT1 (Fig. 6) suggests potential involvement in intracellular transport mechanisms or interactions with ER-associated proteins. This is consistent with the dynamic interplay between cytoplasmic and ER functions in cellular signaling pathways (Liu and Li, 2019). Based on these results, *LaLrHp*NMT1 likely catalyzes the final step of galanthamine synthesis at the cytosol-ER interface in Amaryllidaceae cells, where other pathway enzymes are produced and localized (Fig. 8).

CNMTs are a well-known group of enzymes in the BIA pathway, which are characterized by several phylogenetically distinct plant families [39, 49, 58]. In almost all of them, the primary substrates are *(S)*- or *(R)*- coclaurine, while there are other BIA substrates [58]. The observed substrate promiscuity of *LaLrHp*NMT1 (Fig. 5) aligns with several reports on CNMTs from various plant species (Morris and Facchini, 2019). For example, CNMTs from *E. sinica* catalyze *N*-methylation across structurally diverse compounds, including phenylalkylamines, tryptamine alkaloids, tetrahydroisoquinoline alkaloids, β-carboline, and BIAs (Morris et al., 2018). Similarly, CNMT2 from *Stephania intermedia* exhibits broad specificity, catalyzing the *N*-methylation of norcoclaurine, *N*-methylnorcoclaurine, *N*,*N*-dimethylnorcoclaurine, and magnocurarine (Zhao et al., 2020). The CNMT from *L. chinense* catalyzes methylation of coclaurine, *N*-methylcoclaurine, norarmepavine and armepavine (Zhao et al., 2020; Cheng et al., 2022). Conversely, some CNMTs, such as those from *N. nucifera*, display higher substrate specificity, only methylating nuciferine among ten tested isoquinoline, BIA, and aporphine alkaloids (Chen et al., 2024). Here, we report a few novel reactions catalyzed by CNMT-like NMTs, which are involved in a different alkaloid biosynthetic pathway than BIA. The ability of *LaLrHp*NMT1 to methylate pathway precursors such as tyramine and 3′-*O*-methylnorbelladine suggests a potential role in additional biochemical steps of AA biosynthesis, maybe towards belladine-type AAs (Fig. 1). This broad specificity may reflect an adaptive advantage, allowing plants to fine-tune alkaloid biosynthesis by expanding the range of intermediates available for downstream modification.

Studies in other plant species have shown that *NMT* expression responds dynamically to environmental challenges, consistent with our findings in *H. papilio* shoot cultures under various stress conditions (Fig. 7). For example, salinity, drought, and wounding stressors have

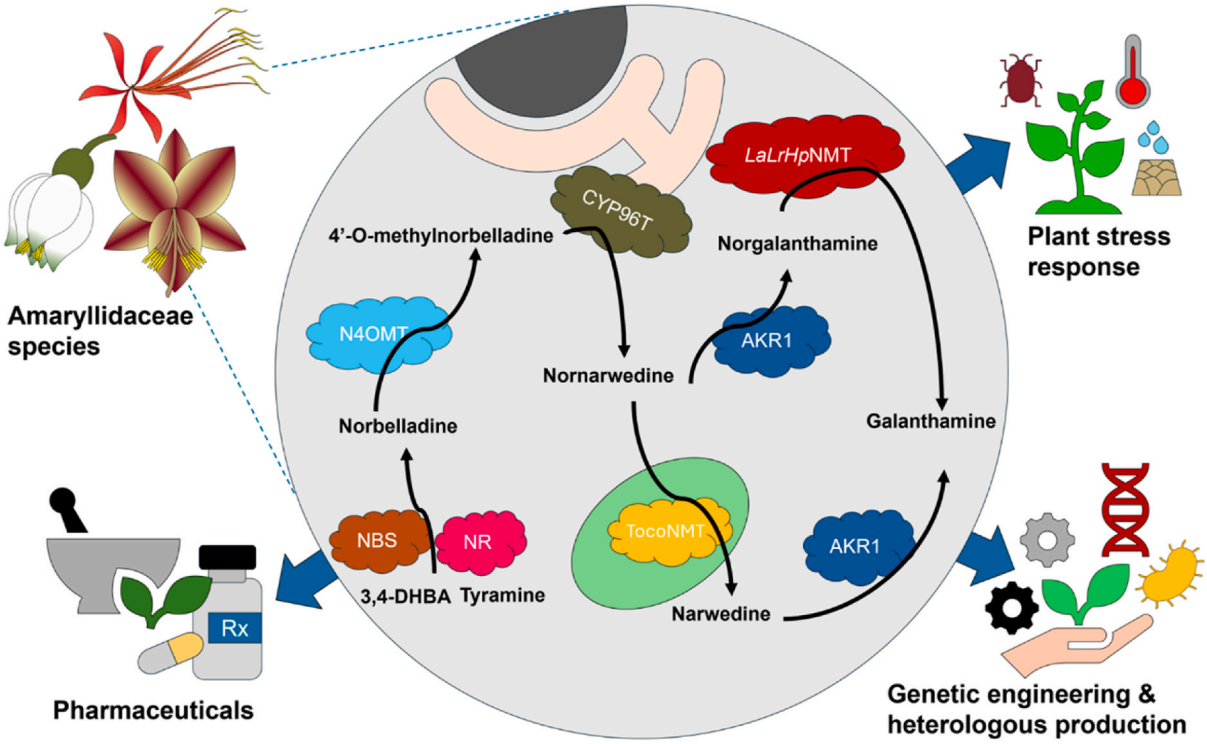

Fig. 8. Schematic representation of galanthamine biosynthesis and translational potential in Amaryllidaceae species. This integrative model highlights the enzymatic steps, subcellular localization, and biotechnological implications of galanthamine biosynthesis. **Top left**: Representative Amaryllidaceae species (*Leucojum aestivum*, *Lycoris radiata*, *Hippeastrum papilio*) used in this study which naturally produce galanthamine. **Center**: A magnified schematic of a plant cell illustrating the subcellular distribution of biosynthetic enzymes. Cytosolic enzymes are shown freely in the cytoplasm; *LaLrHp*NMT and other biosynthetic enzymes (NBS, NR, N4OMT, AKR1) catalyze sequential reactions. CYP96T, a cytochrome P450 enzyme, is localized on the cytosolic face of the endoplasmic reticulum (ER) membrane, while a putative chloroplast-localized TocoNMT is also depicted, suggesting possible plastidial involvement. Black arrows indicate the direction of metabolic flow toward galanthamine. **Outer panels**: Blue arrows point to downstream implications: regulation by plant stress responses, potential for genetic/metabolic engineering & heterologous production, and pharmaceutical relevance (e.g. for treating Alzheimer's disease). (For interpretation of the references to colour in this figure legend, the reader is referred to the Web version of this article.)

been reported to up-regulate expression of *NMT* involved in caffeine biosynthesis, potentially helping the plant defense mechanisms and the regulation of key metabolites for stress resilience (Zhou et al., 2020). Similarly, MeJA, a key mediator of plants' responses to biotic and abiotic stresses, has been shown to up-regulate *NBS* in *L. longituba* while down-regulating *CYP96T1* (Li et al., 2021; Jan et al., 2021). Other Amaryllidaceae-related enzymes, such as *O*-methyltransferases, also exhibit stress-responsive expression patterns (Sun et al., 2018; Li et al., 2021; Koirala et al., 2023). In *Lycoris aurea* roots, cold (4 °C), SNP, MeJA, PEG, and NaCl treatments up-regulated *norbelladine 4′-OMT* expression, whereas abscisic acid down-regulated it. The observed up-regulation of *OMT* (Sun et al., 2018; Li et al., 2021) and *NMT* (present study) under stress conditions suggests a broader role for methyltransferases in modulating biosynthetic pathways in response to environmental cues, potentially aiding plant protection. The targeted alkaloid analysis also supports this idea. Although the correlation between galanthamine and relative *NMT* expression was not evident, some treatments like MeJA and coronatine increased galanthamine production compared to the controls. Another *N*-methylated AA, i.e., narwedine, strongly correlated with the *NMT* expression. This could be due to the function of each metabolite in response to specific stress conditions. For example, some studies suggest that galanthamine has an antibacterial activity, and coronatine is a bacterial toxin (Ločárek et al., 2015). Our findings indicate that interactions between multiple stress-responsive signaling pathways may fine-tune alkaloid production in the Amaryllidoideae subfamily. Given that specialized metabolites, such as alkaloids, often serve protective functions under stress, our results suggest that NMT may play a role in the plant's adaptive response to high temperatures and other environmental challenges.

Another recently characterized NMT from *Narcissus* cv. Tête-à-Tête, a tocopherol methyltransferase-like named TocoNMT, catalyzed the conversion of nornarwedine to narwedine (Fig. 1), another intermediate in galanthamine biosynthesis but did not *N*-methylate norgalanthamine (Mehta et al., 2024). The proposition of an alternate path towards *N*-methylation is consistent with previous studies indicating that multiple distinct enzymatic routes contribute to galanthamine production (Eichhorn et al., 1998; Jayawardena et al., 2024). Tissue-specific expression patterns suggest that different pathways might be optimized for distinct plant organs, such as bulbs for storage or leaves for defense. Metabolic flexibility and redundancy allow plants to maintain alkaloid production even if environmental changes or genetic mutations disrupt one pathway. Evolutionary convergence from ancestral enzyme families could have led to the recruitment of different enzymatic routes, while enzyme promiscuity may have facilitated pathway divergence. Additionally, compartmentalizing biosynthetic steps across different organelles and regulating intermediate pools ensure metabolic efficiency. Given galanthamine's potential role in plant defense, having multiple biosynthetic routes may also enhance adaptability to varying biotic pressures, such as herbivore predation or microbial attack. These factors collectively contribute to the evolutionary advantage of maintaining distinct but converging pathways for galanthamine biosynthesis (Fig. 8).

5. Conclusion

In this study, we identified, isolated, and characterized a set of CNMT-like NMTs from three key Amaryllidaceae species. We demonstrate their critical role in the catalysis of norgalanthamine *N*-

methylation, indicating a new and alternative route for galanthamine biosynthesis. These enzymes, particularly *LaLrHp*NMT1, exhibit high structural and functional conservation with known NMTs from BIA pathways and display notable substrate promiscuity. Flexible docking and *in vitro* assays confirmed that *LaLrHp*NMT1 catalyzes the *N*-methylation of norgalanthamine—a pivotal step in galanthamine production—and that subtle amino acid variations can significantly affect catalytic efficiency. Moreover, subcellular localization studies placed *LaLrHp*NMT1 at the cytosol-ER interface, suggesting a coordinated role with other biosynthetic enzymes in these cellular compartments. Our investigation into the stress-responsive expression of NMTs further indicates that environmental cues, such as heat, salinity, and chemical elicitors like MeJA, modulate the expression of these enzymes. This dynamic regulation likely contributes to the adaptive capacity of plants by fine-tuning alkaloid biosynthesis in response to fluctuating environmental conditions. Such plasticity underpins the evolutionary advantage of maintaining multiple enzymatic pathways for galanthamine synthesis and opens avenues for metabolic engineering aimed at sustainable galanthamine production. Collectively, our results deepen the understanding of the molecular and biochemical underpinnings of alkaloid biosynthesis in Amaryllidaceae and highlight the potential of leveraging these insights to enhance the production of valuable specialized metabolites for pharmaceutical applications. Future research focusing on the regulatory networks and protein-protein interactions at the cytosol-ER interface may further elucidate the integration of these pathways and inform strategies for biotechnological intervention.

Declaration of competing interest

The authors declare the following financial interests/personal relationships which may be considered as potential competing interests: Isabel Desgagne-Penix reports financial support was provided by Canada Research Chairs Program. Isabel Desgagne-Penix reports financial support was provided by Natural Sciences and Engineering Research Council of Canada. If there are other authors, they declare that they have no known competing financial interests or personal relationships that could have appeared to influence the work reported in this paper.

Acknowledgements

The authors thank lab mates Dr. Karen Cristine Goncalves dos Santos, Dr. Manoj Koirala, Dr. Narimane Fradj, and Dr. Bharat Bhusan Majhi for their valuable input and contributions. We also thank Mélodie B. Plourde, Dr. Snehi Gazal, and Prof. Hugo Germain (Université du Québec à Trois-Rivières, QC, Canada) for the sub-cellular localization vectors for assisting with the confocal microscopy. Warm thanks to Xiwei Chen (China) for providing *Lycoris radiata* bulbs and Prof. Antonio Evidente (Institute of Biomolecular Chemistry, National Research Council, Via Campi Flegrei, Pozzuoli, NA, Italy) for providing some alkaloid standards. While preparing this work, the authors used ChatGPT version 4.0, a free AI language model, and Grammarly to correct grammatical errors and enhance readability. After using these tools, the authors reviewed and edited the content as needed and took full responsibility for the publication's content. This research was funded by Canada Research Chair on plant specialized metabolism Award No CRC-2018-00137 to I.D-P. Thanks are extended to the Canadian taxpayers and the Canadian government for supporting the Canada Research Chairs Program. Additional support from the the Natural Sciences and Engineering Research Council of Canada (NSERC) award number RGPIN/3218-2021 to IDP. This work was also supported by the NSERC award number EQPEQ 472990-2015 (Research tools and instruments) for the acquisition of the rt-qPCR and the Canada Foundation for Innovation program John R. Evans Leaders Fund for the acquisition of the LC-qqq-MS.

Appendix A. Supplementary data

Supplementary data to this article can be found online at https://doi.org/10.1016/j.plaphy.2025.110067.

Data availability

Data will be made available on request.

References

Abramson, J., Adler, J.s, Dunger, J., Evans, R., Green, T., Pritzel, A., Ronneberger, O., Willmore, L., Ballard, J., Bambrick, J., Bodenstein, S.W., Evans, D.A., Hung, C., O'Neill, M., Reiman, D., Tunyasuvunakool, K., Wu, Z., Žemgulytė, A., Arvaniti, E., Beattie, C., Bertolli, O., Cherepanov Bridgland, A., Congreve, M., Cowen-Rivers, A.I., Cowie, A., Figurnov, M., Fuchs, F.B., Gladman, H., Jain, R., Khan, Y.A., Low, C.M.R., Perlin, K., Potapenko, A., Savy, P., Singh, S., Stecula, A., Thillaisundaram, A., Tong, C., Yakneen, S., Zhong, E.D., Zielinski, M., Žídek, A., Bapst, V., Kohli, P., Jaderberg, M., Hassabis, D., Jumper, J.M., 2024. Accurate structure prediction of biomolecular interactions with AlphaFold 3. Nature 630, 493–500.

Adasme, M.F., L Linnemann, K., Bolz, S.N., Kaiser, F., Salentin, S., Haupt, V.J., Schroeder, M., 2021. Plip 2021: expanding the scope of the protein–ligand interaction profiler to DNA and RNA. Nucleic Acids Res. 49, W530–W534.

Ali, A.H.M., Abdelrahman, E., Magdi, A., 2019. Alkaloid role in plant defense response to growth and stress. Bioactive Molecules in Plant Defense: Signaling in Growth and Stress, pp. 145–158.

Bennett, M.R., L Thompson, M., A Shepherd, S., S Dunstan, M., J Herbert, A., M Smith, D. R., A Cronin, V., K Menon, B.R., Levy, C., Micklefield, J., 2018a. Structure and biocatalytic scope of coclaurine n-methyltransferase. Angew. Chem. Int. Ed. 57, 10600–10604.

Bennett, M.R., Thompson, M.L., Shepherd, S.A., Dunstan, M.S., Herbert, A.J., Smith, D.R. M., Cronin, V.A., Menon, B.R.K., Levy, C., Micklefield, J., 2018b. 'Structure and Biocatalytic Scope of Coclaurine N-Methyltransferase'. Angew Chem. Int. Ed. Engl. 57, 10600–10604.

Berkov, S., Georgieva, L., Sidjimova, B., Bastida, J., 2022. 'Evaluation of Hippeastrum papilio (Ravenna) Van Scheepen potential as a new industrial source of galanthamine'. Ind. Crop. Prod. 178, 114619.

Berkov, S., Osorio, E., Viladomat, F., Bastida, J., 2020. 'Chemodiversity, chemotaxonomy and chemoecology of Amaryllidaceae alkaloids'. Alkaloids - Chem. Biol. 83, 113–185.

Chen, Sha, Wang, Zhennan, Dong, GangQiang, Zhao, Hedi, Zhu, Yongping, Liu, Yan, Yuan, Ling, Jiang, Jinzhu, Liu, XianJu, Liu, An, 2024. Characterization and molecular engineering of a N-Methyltransferase from edible Nelumbo nucifera leaves involved in nuciferine biosynthesis. J. Agric. Food Chem. 72 (4), 22926–22938.

Cheng, W., Yao, Y., Wang, Q., Chang, X., Shi, Z., Fang, X., Chen, F., Chen, S., Zhang, Y., Zhang, F., 2022. Characterization of benzylisoquinoline alkaloid methyltransferases in Liriodendron chinense provides insights into the phylogenic basis of angiosperm alkaloid diversity. Plant J. 112, 535–548.

Desgagné-Penix, I., 2021. Biosynthesis of alkaloids in Amaryllidaceae plants: a review. Phytochem. Rev. 20, 409–431.

Desgagne-Penix, I., Lamichhane, B., Gélinas, S., Merindol, N., Koirala, M., dos Santos, K. C.G., Germain, H., 2024. Elucidating the Enzyme Network Driving Amaryllidaceae Alkaloids Biosynthesis.

Dethier, M., De Luca, V., 1993. Partial purification of an N-methyltransferase involved in vindoline biosynthesis in Catharanthus roseus. Phytochemistry 32, 673–678.

Ding, Y., Qu, D., Zhang, K.M., Cang, X.X., Kou, Z.N., Xiao, W., Zhu, J.B., 2017. 'Phytochemical and biological investigations of Amaryllidaceae alkaloids: a review'. J. Asian Nat. Prod. Res. 19, 53–100.

Eichhorn, J., Takada, T., Kita, Y., Zenk, M.H., 1998. 'Biosynthesis of the Amaryllidaceae alkaloid galanthamine'. Phytochemistry 49, 1037–1047.

Facchini, P.J., St-Pierre, B., 2005. 'Synthesis and trafficking of alkaloid biosynthetic enzymes'. Curr. Opin. Plant Biol. 8, 657–666.

Girard, Marie-Pierre, Karimzadegan, Vahid, Héneault, Marianne, Cloutier, Francis, Bérubé, Gervais, Berthoux, Lionel, Mérindol, Natacha, Desgagné-Penix, Isabel, 2022. Chemical synthesis and biological activities of Amaryllidaceae alkaloid norbelladine derivatives and precursors. Molecules 27, 5621.

Hagel, J.M., Facchini, P.J., 2012. Subcellular localization of sanguinarine biosynthetic enzymes in cultured opium poppy cells. Cell Dev. Biol. Plant 48, 233–240.

He, M., Qu, C., Gao, O., Hu, X., Hong, X., 2015. Biological and pharmacological activities of Amaryllidaceae alkaloids. RSC Adv. 5, 16562–16574.

Heinrich, M., Lee Teoh, H., 2004. Galanthamine from snowdrop–the development of a modern drug against Alzheimer's disease from local Caucasian knowledge. J. Ethnopharmacol. 92, 147–162.

Herrington, Noah B., Kellogg, Glen E., 2021. 3D interaction homology: computational titration of aspartic acid, glutamic acid and histidine can create pH-tunable hydropathic environment maps. Front. Mol. Biosci. 8, 773385.

Hotchandani, T., Desgagne-Penix, I., 2017. Heterocyclic amaryllidaceae alkaloids: biosynthesis and pharmacological applications. Curr. Top. Med. Chem. 17, 418–427.

Irwin, J.J., Tang, K.G., Young, J., Dandarchuluun, C., Wong, B.R., Khurelbaatar, M., Moroz, Y.S., Mayfield, J., Sayle, R.A., 2020. 'ZINC20-A Free Ultralarge-Scale Chemical Database for Ligand Discovery'. J. Chem. Inf. Model. 60, 6065–6073.

Jan, R., Asaf, S., Numan, M., Kim, K., 2021. Plant secondary metabolite biosynthesis and transcriptional regulation in response to biotic and abiotic stress conditions. Agronomy 11, 968.
Jayawardena, T.U., Merindol, N., Liyanage, N.S., Desgagne-Penix, I., 2024. Unveiling amaryllidaceae alkaloids: from biosynthesis to antiviral potential - a review. Nat. Prod. Rep. 41, 721–747.
Ka, S., Koirala, M., Merindol, N., Desgagne-Penix, I., 2020. 'Biosynthesis and Biological Activities of Newly Discovered Amaryllidaceae Alkaloids'. Molecules 25, 4901.
Karimzadegan, Vahid, Koirala, Manoj, Sobhanverdi, Sajjad, Merindol, Natacha, Majhi, Bharat Bhusan, Gélinas, Sarah-Eve, Timokhin, Vitaliy I., Ralph, John, Dastmalchi, Mehran, Desgagné-Penix, Isabel, 2024. Characterization of cinnamate 4-hydroxylase (CYP73A) and p-coumaroyl 3′-hydroxylase (CYP98A) from Leucojum aestivum, a source of Amaryllidaceae alkaloids. Plant Physiol. Biochem. 210, 108612.
Kilgore, M.B., Augustin, M.M., May, G.D., Crow, J.A., Kutchan, T.M., 2016. 'CYP96T1 of Narcissus sp. aff. pseudonarcissus Catalyzes Formation of the Para-Para' C-C Phenol Couple in the Amaryllidaceae Alkaloids'. Front. Plant Sci. 7, 225.
Kilgore, Matthew B., Augustin, Megan M., Starks, Courtney M., Neil-Johnson, Mark O., May, Gregory D., Crow, John A., Kutchan, Toni M., 2014. Cloning and characterization of a norbelladine 4′-O-Methyltransferase involved in the biosynthesis of the alzheimer's drug galanthamine in Narcissus sp. aff. pseudonarcissus. PLoS One 9, e103223.
Kilgore, Matthew B., Holland, Cynthia K., Jez, Joseph M., Kutchan, Toni M., 2016. Identification of a noroxomaritidine reductase with amaryllidaceae alkaloid biosynthesis related activities. J. Biol. Chem. 291, 16740–16752.
Koirala, M., Merindol, N., Karimzadegan, V., Gelinas, S.E., Liyanage, N.S., Lamichhane, B., Tobon, M.C.G., Lague, P., Desgagne-Penix, I., 2024. 'Kinetic and in silico structural characterization of norbelladine O-methyltransferase of Amaryllidaceae alkaloids biosynthesis'. J. Biol. Chem. 300, 107649.
Koirala, Manoj, dos Santos, Karen Cristine Goncalves, Gélinas, Sarah-Eve, Ricard, Simon, Karimzadegan, Vahid, Lamichhane, Basanta, Liyanage, Nuwan Sameera, Merindol, Natacha, Desgagné-Penix, Isabel, 2023. Auxin and light-mediated regulation of growth, morphogenesis, and alkaloid biosynthesis in Crinum x powellii 'Album' callus. Phytochemistry 216, 113883.
Koirala, Manoj, Karimzadegan, Vahid, Sameera Liyanage, Nuwan, Mérindol, Natacha, Desgagné-Penix, Isabel, 2022. Biotechnological approaches to optimize the production of Amaryllidaceae alkaloids. Biomolecules 12, 893.
Lamichhane, B., Gelinas, S.E., Merindol, N., Koirala, M., Dos Santos, K.C.G., Germain, H., Desgagne-Penix, I., 2025. Elucidating the enzyme network driving Amaryllidaceae alkaloids biosynthesis in Leucojum aestivum. Plant Biotechnol. J. doi: 10.1111/pbi.70026. Online ahead of print.
Lee, S., Park, N.I., Park, Y., Park, K.C., Kim, E.S., Son, Y.K., Choi, B.S., Kim, N.S., Choi, I. Y., 2024. O- and N-Methyltransferases in benzylisoquinoline alkaloid producing plants. Genes Genomics 46, 367–378.
Li, Q., Xu, J., Zheng, Y., Zhang, Y., Cai, Y., 2021. 'Transcriptomic and Metabolomic Analyses Reveals That Exogenous Methyl Jasmonate Regulates Galanthamine Biosynthesis in Lycoris longituba Seedlings'. Front. Plant Sci. 12, 713795.
Li, W., Qiao, C., Pang, J., Zhang, G., Luo, Y., 2019. The versatile O-methyltransferase LrOMT catalyzes multiple O-methylation reactions in Amaryllidaceae alkaloids biosynthesis. Int. J. Biol. Macromol. 141, 680–692.
Liscombe, D.K., Usera, A.R., O'Connor, S.E., 2010. Homolog of tocopherol C methyltransferases catalyzes N methylation in anticancer alkaloid biosynthesis. Proc. Natl. Acad. Sci. U. S. A. 107, 18793–18798.
Liu, L., Li, J., 2019. 'Communications between the endoplasmic reticulum and other organelles during abiotic stress response in plants'. Front. Plant Sci. 10, 749.
Liu, Z., Sun, B., Li, J., Xiang, Y., Wang, R., Jiang, X., Zhu, X., Xu, S., Wang, R., 2024. Functional characterization of CYP96T1-like cytochrome P450 from Lycoris aurea catalyzing para-para' and para-ortho' oxidative coupling in amaryllidaceae alkaloids biosynthesis. Front. Plant Sci. 15, 1438102.
Ločárek, Miroslav, Nováková, Jitka, Klouček, Pavel, Hošťálková, Anna, Kokoška, Ladislav, Gábrlová, Lucie, Šafratová, Marcela, Opletal, Lubomír, Cahlíková, Lucie, 2015. Antifungal and antibacterial activity of extracts and alkaloids of selected Amaryllidaceae species. Nat. Prod. Commun. 10, 1934578X1501000912.
Loy, C., Schneider, L., 2006. Galantamine for Alzheimer's disease and mild cognitive impairment. Cochrane Database Syst. Rev. 2006, CD001747.
Majhi, B.B., Gélinas, S.E., Mérindol, N., Ricard, S., Desgagné-Penix, I., 2023. Characterization of norbelladine synthase and noroxomaritidine/norcraugsodine reductase reveals a novel catalytic route for the biosynthesis of Amaryllidaceae alkaloids including the Alzheimer's drug galanthamine. Front. Plant Sci. 14, 1231809.
Mehta, N., Meng, Y., Zare, R., KamenetskyGoldstein, R., Sattely, E., 2024. A developmental gradient reveals biosynthetic pathways to eukaryotic toxins in monocot geophytes. Cell 187, 5620–5637.
Merindol, N., Belem Martins, L.L., Elfayres, G., Custeau, A., Berthoux, L., Evidente, A., Desgagne-Penix, I., 2024. Amaryllidaceae alkaloids screen unveils potent anticoronaviral compounds and associated structural determinants. ACS Pharmacol. Transl. Sci. 7, 3527–3539.
Morris, J.S., Facchini, P.J., 2019. Molecular origins of functional diversity in benzylisoquinoline alkaloid methyltransferases. Front. Plant Sci. 10, 1058.
Morris, J.S., Groves, R.A., Hagel, J.M., Facchini, P.J., 2018. An N-methyltransferase from Ephedra sinica catalyzing the formation of ephedrine and pseudoephedrine enables microbial phenylalkylamine production. J. Biol. Chem. 293, 13364–13376.
Morris, J.S., Yu, L., Facchini, P.J., 2020. 'A single residue determines substrate preference in benzylisoquinoline alkaloid N-methyltransferases'. Phytochemistry 170, 112193.
Okonechnikov, K., Golosova, O., Fursov, M., Ugene team, 2012. Unipro UGENE: a unified bioinformatics toolkit. Bioinformatics 28, 1166–1167.
Olin, J., Schneider, L., 2002. Galantamine for Alzheimer's disease. Cochrane Database Syst. Rev., CD001747
Orhan, Ilkay Erdogan, Sezer Senol Deniz, F., Eren, Gokcen, Sener, Bilge, 2021. Molecular approach to promising cholinesterase inhibitory effect of several Amaryllidaceae alkaloids: further re-investigation. South Afr. J. Bot. 136, 175–181.
Ptak, A., Morańska, E., Saliba, S., Zieliński, A., Simlat, M., Laurain-Mattar, D., 2016. Elicitation of galanthamine and lycorine biosynthesis by Leucojum aestivum L. and L. aestivum 'Gravety Giant' plants cultured in bioreactor RITA®. Plant Cell Tissue Organ Cult. 128, 335–345.
Ptak, A., Moranska, E., Skrzypek, E., Warchol, M., Spina, R., Laurain-Mattar, D., Simlat, M., 2020. Carbohydrates stimulated Amaryllidaceae alkaloids biosynthesis in Leucojum aestivum L. plants cultured in RITA((R)) bioreactor. PeerJ 8, e8688.
Rønsted, N., Symonds, M.R.E., Birkholm, T., Christensen, S.B., Meerow, A.W., Molander, M., Mølgaard, P., Petersen, G., Rasmussen, N., Van Staden, J., 2012. Can phylogeny predict chemical diversity and potential medicinal activity of plants? A case study of Amaryllidaceae. BMC Evol. Biol. 12, 1–12.
Singh, A., Massicotte, M.A., Garand, A., Tousignant, L., Ouellette, V., Berube, G., Desgagne-Penix, I., 2018. 'Cloning and characterization of norbelladine synthase catalyzing the first committed reaction in Amaryllidaceae alkaloid biosynthesis'. BMC Plant Biol. 18, 338.
Sun, B., Wang, P., Wang, R., Li, Y., Xu, S., 2018. Molecular cloning and characterization of a meta/para-O-Methyltransferase from Lycoris aurea. Int. J. Mol. Sci. 19, 1911.
Tousignant, L., Diaz-Garza, A.M., Majhi, B.B., Gelinas, S.E., Singh, A., Desgagne-Penix, I., 2022. Transcriptome analysis of *Leucojum aestivum* and identification of genes involved in norbelladine biosynthesis. Planta 255, 30.
Wang, N., Shu, X., Zhang, F., Song, G., Wang, Z., 2024. Characterization of the heat shock transcription factor family in Lycoris radiata and its potential roles in response to abiotic stresses. Plants 13, 271.
Zhao, W., Shen, C., Zhu, J., Ou, C., Liu, M., Dai, W., Liu, X., Liu, J., 2020. Identification and characterization of methyltransferases involved in benzylisoquinoline alkaloids biosynthesis from Stephania intermedia. Biotechnol. Lett. 42, 461–469.
Zhou, M.Z., Yan, C.Y., Zeng, Z., Luo, L., Zeng, W., Huang, Y.H., 2020. 'N-Methyltransferases of Caffeine Biosynthetic Pathway in Plants'. J. Agric. Food Chem. 68, 15359–15372.